

Advanced Functional Materials

Silicon-based Laser Desorption Ionization Mass Spectrometry for the Analysis of Biomolecules: A Progress Report --Manuscript Draft--

Manuscript Number:	
Full Title:	Silicon-based Laser Desorption Ionization Mass Spectrometry for the Analysis of Biomolecules: A Progress Report
Article Type:	Progress Report
Section/Category:	
Keywords:	silicon nanostructures; Surface functionalization; laser desorption ionization (LDI); mass spectrometry imaging (MSI).
Corresponding Author:	Pere Ràfols Universitat Rovira i Virgili Tarragona, SPAIN
Additional Information:	
Question	Response
Please submit a plain text version of your cover letter here.	<p>Dear Editor,</p> <p>Please find attached the manuscript "Silicon-based Laser Desorption Ionization Mass Spectrometry for the Analysis of Biomolecules: A Progress Report" co-authored by Stefania-Alexandra Iakab, Pere Ràfols, María García-Altares, Oscar Yanes and Xavier Correig to be considered for publication as a Progress Report in the Advanced Functional Materials journal. Here, we present recent developments on silicon-based LDI approaches for mass spectrometry analysis of biomolecules. The facility of fabrication and surface functionalization of silicon-based substrates open a completely new chapter in the field of mass spectrometry imaging and in particular in the detection of low mass compounds. Since the first silicon-based substrate was introduced as desorption/ionization on silicon (Siuzdak et al, Nature, 1999), the number of papers published on designing and fabricating silicon nanostructures for LDI-MS has grown rapidly, with more than 100 papers published in the last 10 years, proving that is really an emerging research field. Our report will focus on the existing fabrication processes, functionalization techniques and practical applications of porous silicon and silicon nanostructures for LDI-MS. The report will also include a detailed revision on the current nanotechnology used to create silicon-based substrates with the essential requirements for an optimal LDI analysis by providing an overview of the ionization and desorption mechanisms in the interplay of the analyte with the silicon nanostructure and the laser. This progress report is intended to be useful for materials scientists or any experimentalist researcher familiar with nanotechnology and mass spectroscopy who needs to detect or maximise the detection of biomolecules using nanostructured silicon surfaces for targeted or untargeted analysis.</p> <p>All authors are aware and agree to the submission of the manuscript to the Advanced Functional Materials journal. I confirm that neither the manuscript nor any parts of its content are currently under consideration or published in another journal.</p> <p>Looking forward to hearing from you. Yours sincerely,</p>

	Dr. Pere Ràfols Soler
Do you or any of your co-authors have a conflict of interest to declare?	No. The authors declare no conflict of interest.
Corresponding Author Secondary Information:	
Corresponding Author's Institution:	Universitat Rovira i Virgili
Corresponding Author's Secondary Institution:	
First Author:	Stefania Alexandra Iakab
First Author Secondary Information:	
Order of Authors:	Stefania Alexandra Iakab
	Pere Ràfols
	María García-Altres
	Oscar Yanes
	Xavier Correig
Order of Authors Secondary Information:	
Abstract:	<p>Matrix-assisted laser desorption/ionization mass spectrometry (MALDI-MS) is widely used in the biomedical field for the label-free analysis of molecules such as drugs, lipids, peptides, and proteins. MALDI-MS can also perform Imaging experiments to map simultaneously the concentration of hundreds of compounds on biological tissues. However, the great potential of MALDI-MS Imaging for untargeted in-situ metabolomics has not been exploited yet, since organic matrices used in traditional MALDI-MS applications introduce excessive interferences in the low m/z range. For this reason, nanostructured materials and in particular silicon-based LDI strategies have become a strong alternative, since they provide a much weaker background. Herein, we review the recent developments in fabrication, functionalization and practical applications of silicon-based LDI-MS methods. We also report the basic requirements of silicon-based substrates for an optimal LDI analysis by providing an overview of the LDI mechanisms using silicon-based substrates instead of organic matrices. Finally, the extensive potential of silicon-based substrates is discussed, giving suggestions on topics of interest for future research.</p>

**Silicon-based Laser Desorption Ionization Mass Spectrometry for the Analysis of
Biomolecules: A Progress Report**

Stefania Alexandra Iakab, Pere Rafols, María García-Altres, Oscar Yanes, Xavier Correig*

Dr. Pere Rafols

Department of Electronic Engineering, Rovira i Virgili University, IISPV, Tarragona, 43007,
Spain

Spanish Biomedical Research Centre in Diabetes and Associated Metabolic Disorders
(CIBERDEM), Madrid, 28029, Spain

Email: pere.rafols@urv.cat

Keywords: silicon nanostructures, surface functionalization, laser desorption ionization (LDI),
mass spectrometry imaging (MSI)

Abstract

1 Matrix-assisted laser desorption/ionization mass spectrometry (MALDI-MS) is widely used in
2
3 the biomedical field for the label-free analysis of molecules such as drugs, lipids, peptides, and
4
5 proteins. MALDI-MS can also perform Imaging experiments to map simultaneously the
6
7 concentration of hundreds of compounds on biological tissues. However, the great potential of
8
9 MALDI-MS Imaging for untargeted in-situ metabolomics has not been exploited yet, since
10
11 organic matrices used in traditional MALDI-MS applications introduce excessive interferences
12
13 in the low m/z range. For this reason, nanostructured materials and in particular silicon-based
14
15 LDI strategies have become a strong alternative, since they provide a much weaker background.
16
17 Herein, we review the recent developments in fabrication, functionalization and practical
18
19 applications of silicon-based LDI-MS methods. We also report the basic requirements of
20
21 silicon-based substrates for an optimal LDI analysis by providing an overview of the LDI
22
23 mechanisms using silicon-based substrates instead of organic matrices. Finally, the extensive
24
25 potential of silicon-based substrates is discussed, giving suggestions on topics of interest for
26
27 future research.
28
29
30
31
32
33
34
35
36
37
38
39
40
41
42
43
44
45
46
47
48
49
50
51
52
53
54
55
56
57
58
59
60
61
62
63
64
65

1. Introduction

1
2 Matrix-assisted laser desorption/ionization mass spectrometry (MALDI MS) is one of the most
3
4 versatile mass spectrometry analysis techniques that can detect a wide range of molecules in
5
6 complex biological samples. It can be used to detect chemical compounds in liquid samples (i.e.
7
8 urine, serum, etc.), but the great advantage of this technique is its ability to map the
9
10 concentration of chemical compounds over an animal or vegetal surface. The molecular images
11
12 obtained correlate spatially with the morphology of such tissues.^[1-4]
13
14

15
16 Traditionally, MALDI implies the use of an organic matrix deposited onto the sample for laser
17
18 desorption/ionization. The requirements of a successful MALDI matrix are high optical
19
20 absorption at the laser irradiation wavelength, good analyte incorporation into the matrix,
21
22 available proton donor or acceptor for an efficient ionization and minimal fragmentation of
23
24 analyte.^[3] Two of the most common organic matrices are α -cyano-4-hydroxycinnamic acid
25
26 (CHCA) and 2,5-dihydroxybenzoic acid (DHB).
27
28

29
30 Although organic matrices ionize efficiently a wide variety of molecules, they present some
31
32 important limitations:
33
34

- 35
36 • The use of an organic matrix hampers the analysis in the low mass range due to the presence
37
38 of many background ion signals generated from the organic matrix clusters.^[5] This results
39
40 in major disadvantages for the use of MALDI-MS in metabolomics.
41
42
- 43
44 • Inhomogeneity in the co-crystallization of the organic matrix with the analyte leads to a
45
46 lack of reproducibility. The dried organic matrix crystals vary in size and shape across the
47
48 surface, leading to differences in pixel-to-pixel MS signals intensities, thus making difficult
49
50 quantitative MALDI analysis.^[5]
51
52
- 53
54 • Although a wide range of commercially organic matrices is available, its selection and
55
56 deposition optimization are a manual and complex process. Each experiment may require
57
58 a specific matrix which has to be optimized, and in some cases, chemical interactions
59
60 between analyte and matrix may occur.^[2]
61
62

- Poor lateral resolution is frequently associated with the presence of matrix. This is mainly caused by heterogeneous co-crystallization of the matrix and analyte. Additionally, the solvent often interacts with tissues and induces delocalization of molecules.^[6] This issue was partially solved by finely controlled matrix deposition methods.^[3]

To overcome heterogeneous co-crystallization between matrix and analyte during spray-coating, organic matrices were deposited uniformly and homogeneously directly onto analytes via sublimation method.^[7] This method improves the lateral resolution, but given the long acquisition times needed in tissue imaging, the matrix may evaporate during measurement, rendering this approach hardly applicable.^[8] Comparing the two deposition methods, spray-coating results in higher analyte extraction efficiency (i.e., increased sensitivity) whereas sublimation improves lateral resolution.^[7]

In the quest to find alternatives to organic matrices deposited over the sample, scientific efforts turned to substrates that could promote the ionization and desorption of compounds without introducing exogenous material that could interfere with the detection of endogenous compounds. As a consequence, new solid-state substrate materials have been developed and used. Several reviews ^[5,9–12] have described the use of inorganic materials based on carbon, silicon, metals or metal-oxides that have been used extensively in LDI-MS applications as substitutes of the organic matrices. These materials have the main function to promote the ionization and desorption processes of the compounds. They have to be stable under vacuum, to absorb the laser irradiation and to not cause ion interferences in the low mass range of the spectra. Moreover, other properties such as low thermal conductivity, high electrical conductivity and high surface area to volume ratio may be considered for an efficient LDI process.^[13] They are synthesized as nanoparticles or nanostructured surfaces in order to enhance the absorption at UV and have a high area/volume ratio. The use of metallic

nanoparticles, especially noble metals ^[14–16], metal oxide nanoparticles ^[17], and silicon- and carbon-based substrates as nanostructured surfaces ^[11,18], are under rigorous investigation.

Silicon presents a clear advantage over other alternatives as it is a versatile material with huge potential for the development of a large number of applications. Its properties such as chemical stability, high thermal conductivity, excellent biocompatibility, rich abundance, unique electronic, optical, and mechanical properties, have established silicon as a ubiquitous material widely used in biomedical applications.^[19,20] From the technological point of view, the microelectromechanical systems industry has developed advanced technologies with huge potential for silicon-based materials. These microelectronic technologies, based on dry high vacuum processes, share the advantage of being able to fabricate highly homogeneous, reliable and repetitive surfaces. Using all these resources, scientists have dedicated time and effort to use intrinsic or functionalized silicon in several forms (porous, nanostructured) as a substrate for LDI-MS applications.^[12]

Silicon-based substrates for matrix-free LDI-MS first appeared in 1998 in the form of porous silicon (pSi) as desorption ionization on silicon (DIOS) technique.^[21] This technique has further developed into nanostructure-initiator mass spectrometry (NIMS) where a fluorinated compound, called initiator, was impregnated into the pSi ^[22] in order to get stability over the surface and have higher ion desorption and ionization yield. Other silicon-based nanostructures have been used as well: silica nanoparticles, silicon nanowires and nanostructured silicon surfaces (ex. nanocone array).^[12]

In this review, we focus on describing the various kinds of silicon-based substrates that were successfully used in all types of LDI-MS experiments. The first section describes the fabrication and application of pSi substrates, mainly based on DIOS and NIMS technologies. The second section describes the fabrication and application of different types of 2D and 3D silicon nanostructures. The third section focuses on the LDI mechanism of each type of substrate in order to give a better understanding of the current technologies and ideologies. Lastly, we

1 discuss important current issues on the silicon substrate technologies for LDI-MS applications
2 and provide guidelines to select the most suitable substrate for LDI-MS experiments for diverse
3 applications.
4
5
6

7 8 **2. Porous Silicon – DIOS MS and NIMS** 9

10 DIOS was first developed by Siuzdak and his group in 1999^[21,23] where silicon was first used
11 as a pSi substrate that traps the analytes deposited on the surface allowing the laser irradiation
12 to vaporize and ionize them. This matrix-free method demonstrated its great value by detecting
13 some compounds such as peptides and small drug molecules at concentrations as low as
14 femtomole and attomole levels and also resulting in little or no fragmentation. Budimir et al..
15 reported using commercial DIOS chip, which was patented by Dr. Gary Siuzdak, from Mass
16 Consortium Corporation (San Diego, CA, USA).^[24]
17
18
19
20
21
22
23
24
25
26

27 28 **2.1. Fabrication of the porous silicon substrate** 29

30 The basic DIOS fabrication process starts from a flat crystalline silicon etched by a simple
31 galvanostatic procedure as described previously by Cullis et al. in 1997.^[25] Basically, n- or p-
32 type silicon wafers can be etched in a solution of ethanol/hydrofluoric acid in the presence of
33 current with or without illumination, depending on the silicon wafer type. The schematic
34 diagram of the electrochemical etching set-up used for pSi fabrication can be seen in the
35 supporting information (see **Figure S1**). This fabrication method has been adjusted by many
36 groups by varying parameters such as pre-etching cleaning methods, current density,
37 ethanol/HF solution concentrations, etching time and illumination (see **Table S1**). In most
38 cases, the electrochemical etching was carried out in custom-built Teflon cells. The typical pSi
39 structure created by the group of Guinan et al.^[26] is illustrated in **Figure 1**. Some groups used
40 the electrochemical etching method on silicon wafers previously patterned with standard
41
42
43
44
45
46
47
48
49
50
51
52
53
54
55
56
57
58
59
60
61
62
63
64
65

1 lithography methods ^[27,28], while others developed a new processing method by combining
2 electrochemical etching and laser processing.^[29]
3

4 To create pSi, unconventional techniques have also been used. Silicon nanocavity arrays with
5 low (9%) or high (92%) porosities have been obtained using an electron beam lithography
6 system for high-resolution nanopatterning, then a reactive ion etching (RIE) protocol was used
7 to create the pSi.^[30] Compared to electrochemically etched surfaces, this method uses dry
8 chemistry that reduces drastically surface contamination and safety risks to the users inherent
9 to the use of HF solutions. Another atypical method for obtaining pSi for DIOS-MS is described
10 by Gaspari et al.^[31] In this study, the pSi was fabricated by coating silicon wafer pieces with a
11 500 nm thick nanoporous film of silicon oxide. Goto et al. used evaporation-induced self-
12 assembly (EISA) method to create mesoporous organosilica films with surface open pores.^[32]
13 The pSi surface was created using an amphiphilic block copolymer as a structure-directing
14 surfactant template for the triphenylamine (TPA)-derived sol-solution that was spin-coated onto
15 the Si substrate. The film was treated with ammonia vapor and heat to obtain a condensed stable
16 siloxane network. Lastly, the surfactant was removed by heating in toluene at elevated
17 temperatures.^[32] However, all fabrication methods for DIOS substrates are incomplete without
18 the stabilization and/or functionalization of the surface.
19
20
21
22
23
24
25
26
27
28
29
30
31
32
33
34
35
36
37
38
39
40
41
42

43 **2.2. Surface modification methods**

44 Porous silicon substrates were developed mainly for the easy detection of low molecular weight
45 molecules by removing unnecessary background signal from the organic matrices. Interestingly,
46 porous silicon together with the organic matrices can have a synergistic effect and provide
47 enhanced signal to detect larger molecules such as peptides and proteins. However, for using
48 pSi substrates, stabilization (or passivation) of pSi is necessary because the freshly etched pSi
49 surface is metastable due to the silicon-hydride terminations. Therefore, the surface energy
50 configuration can be easily affected by neighboring energies, so stabilization processes are
51
52
53
54
55
56
57
58
59
60
61
62
63
64
65

1 applied. One of the most common stabilization processes is the oxidation of the pSi surface.
2 More stabilization methods for pSi are represented in **Table S2**. The stabilized pSi surfaces are
3 resistant to air and other external factors (or environments), they present good longevity with
4 lifetimes greater than 9 months ^[33] and constant DIOS-MS activity over an extended period of
5 time.
6

7
8
9
10
11 Functionalization of a DIOS chip consists in the modification of the pSi surface with functional
12 groups that promote specific bonding between pSi and the analytes in order to enable the
13 detection of certain classes of molecules which cannot be detected otherwise. Also,
14 functionalization methods are used to improve ionization. To achieve this, the pSi surface is
15 first derivatized. The derivatization process results in slight changes in the chemical property
16 of the surface by adding specific derivatization agents. The most common derivatization
17 methods are described below in detail in section *2.1.1. Derivatization*. After the pSi is
18 derivatized, functional groups can be added for specific bonding. The bonding can be designed
19 according to hydrophobic, electrostatic, coordination bond, or Lewis acid-base interactions
20 between functional group and analyte. For example, pSi is commonly functionalized to create
21 antibody-antigen, receptor-enzyme or DNA-protein interactions.^[34] Common
22 functionalization methods are described below in sections *2.1.3.* and *2.1.4.*, and all surface
23 modification methods are represented in **Table 1**.
24
25
26
27
28
29
30
31
32
33
34
35
36
37
38
39
40
41
42
43
44

45 *2.1.1. Derivatization*

46 The most frequently used derivatization method is called silylation and it combines ozone
47 oxidation treatment with hydrosilylation.^[26,33,35,36,38] Essentially, the DIOS chips are oxidized
48 by exposure to ozone plasma and the surface derivatization is finalized with the modification
49 of hydroxyl groups by silylation. Silylating reagents can vary according to the application of
50 the DIOS chip. For instance, Trauger et al. ^[35] derivatized the surface with BSTFA, MSTFA,
51 HMDS, ODMCS, CDOS, APDMES, FHCS, or PFPPDCS that generated trimethylsilyl- (TMS),
52 amine-, C8-, C18-, perfluoroalkyl-, and perfluorophenyl-derivatized surfaces, from which the
53
54
55
56
57
58
59
60
61
62
63
64
65

1 most effective terminal groups proved to be amino- and pentafluorophenyl-. Protein model
2 systems (BSA and hemoglobin tryptic digests), three small drug molecules (Propafenone,
3 verapamil, midazolam), simple neutral carbohydrates (Maltotriose, sucrose) and four amino
4 acids (phenylalanine, alanine, isoleucine/leucine, glutamic acid) were analyzed and detected.
5
6 The hydrophobic perfluorophenyl-derivatized surface is more responsive to hydrophobic
7 molecules while the amine-derivatized surface is more responsive to hydrophilic molecules,
8 demonstrating that silyl derivatization is a flexible approach for preparing functionalized DIOS
9 chips for analyte-specific applications and for the selective adsorption of analytes. The groups
10 in ^[36,37] used the same method to obtain derivatized DIOS chips but in this case, the chips were
11 silanized via the addition of neat silane (pentafluorophenylpropyldimethylchlorosilane,
12 F5PhPr). These chips served to study the distribution of bioactive compounds synthesized in
13 the hypobranchial gland of the marine sea snail, *D. orbita*. Results showed a strong correlation
14 between histological regions and the localization of both known and unknown metabolites. T.
15 Guinan and team ^[26,33,38,39] have also used neat silane (F5PhPr) as silylating agent to detect three
16 illicit drugs: MA, MDMA and cocaine, with detection limits comparable to current
17 techniques.^[33] The same group also detected exogenous and endogenous drug compounds from
18 fingerprints ^[26], using neat BisF17 for high throughput quantitative analysis of methadone in
19 saliva, plasma and urine ^[38] and neat F13 to detect amphetamines, opiates, benzodiazepines and
20 tropane alkaloids at concentrations relevant to body fluid testing.^[39] Other more uncommon
21 derivatization agents were used by Gaspari et al. and Tuomikoski et al.^[31,44] Tuomikoski et al.
22 ^[44] chemically derivatized the pSi samples with 10-undecenoic acid and ethyl undecenoate to
23 obtain organic monolayers covalently attached to the surface by Si–C bonds. With this substrate,
24 they analyzed solutions of midazolam, propranolol, buprenorphine, psilocin, 1-naphthalene
25 methylamine, and 2-naphthylacetic acid, dichloromethylene bisphosphonate and
26 dichloromethyl phosphonate. Results strengthened the analysis method's validity, obtaining
27 detection sensitivity at the 100–150 fmol level for the pharmaceutical compounds. Similarly,
28
29
30
31
32
33
34
35
36
37
38
39
40
41
42
43
44
45
46
47
48
49
50
51
52
53
54
55
56
57
58
59
60
61
62
63
64
65

1 Gaspari et al. ^[31] derivatized their pSi through pentane rinsing to selectively capture three low
2 molecular weight peptides substance P, renin substrate tetrapeptide, and angiotensin to detect
3
4 calcitonin in spiked in human plasma.
5
6
7

9 2.1.2. Nanostructure initiator mass spectrometry (NIMS)

10 DIOS demonstrated such versatility by combining nanoporous surfaces and functionalization
11
12 methods that scientists were inspired to evolve this technique into a new one: nanostructure-
13
14 initiator mass spectrometry (NIMS). NIMS focuses on combining the properties of
15
16 nanostructured materials and fluorinated compounds. This new MS analysis technique uses
17
18 compounds called ‘initiator’ that are trapped in nanostructured surfaces to release and ionize
19
20 intact molecules adsorbed on the surface.^[22] NIMS has to be differentiated from silylated pSi
21
22 since the fluorinated compounds are bound differently. In case of the silylated pSi, the
23
24 fluorinated compounds are chemically bound to the surface while in case of NIMS they are
25
26 physically adsorbed onto the surface. In other words, NIMS has taken advantage of the
27
28 nanostructured surfaces’ ability to trap liquids and it is not using any functionalization methods
29
30 to activate the surface. Most research groups use pSi as nanostructured substrate and Bis17 as
31
32 initiator ^[22,39,43,48,50,54], however, the first reports on using NIMS have studied the use of many
33
34 initiators.^[22,54] Perfluorinated siloxanes are preferred for NIMS because they are effectively
35
36 trapped within the nanostructured surface and have the best performance.
37
38
39

40 The well-known manufacturing process of pSi and easy implementation of initiators has led to
41
42 the successful use of NIMS for various applications. Firstly, the versatility of NIMS was
43
44 demonstrated by Northen et al.^[22] The group tested various initiators for a large number of
45
46 applications: direct analysis of blood and urine, characterization of peptide microarrays,
47
48 detection of endogenous phospholipids of aMDA-MB-231 cancer cell line and MSI analysis of
49
50 mouse embryo tissue. A protocol for preparing and applying NIMS surfaces has been published
51
52 by the same group where they give detailed step by step instructions accompanied by
53
54
55
56
57
58
59
60
61
62
63
64
65

1 supplementary movies.^[22,54] Secondly, NIMS performance was compared with DIOS and
2 (nanostructure assisted laser desorption ionization) NALDI for the detection of four drug
3 classes: amphetamines, benzodiazepines, opiates, and tropane alkaloids.^[39] NIMS produced
4 better LODs for oxycodone in both water and PBS. Lastly, a study on the pSi morphology
5 showed the pore-size-dependent analyte selectivity of NIMS. This selective behavior manifests
6 mainly through physical interactions of analyte molecules and NIMS surfaces. The sensitivity
7 of NIMS is directly affected by the pore and analyte size. In this study, analytes ranging from
8 m/z 175.12 to m/z 3657.92 and substrates of pore size from ~4 to 12 nm (porosity from ~7%
9 to 70%) were analyzed.^[51]

10 Variations on NIMS technology quickly appeared. In the first place, NIMS was modified by
11 use of new augmenting components such as organic matrices or metallic nanoparticles.
12 Moening et al. used a sublimated organic matrix (DHB) together with NIMS to develop a new
13 hybrid ionization approach called matrix-enhanced nanostructure initiator mass spectrometry
14 (ME-NIMS). ME-NIMS improved the performance of conventional NIMS reducing the limit
15 of detection of pentamidine by at least one order of magnitude. This improvement was also seen
16 in the detection of lipids and small drug molecules during tissue imaging.^[48] Patti et al. ^[43]
17 replaced the organic matrix with AgNO₃ coating of the NIMS substrate. The study focused on
18 localizing perturbations in metabolism within pathological tissues by MSI. It demonstrated that
19 deposition of cationization agents (AgNO₃) to the NIMS surface allows imaging of otherwise
20 difficult sterol molecules such as cholesterol. Lastly, NIMS was modified by redesigning the
21 nanostructured silicon. For this, the highly dangerous electrochemical etching of silicon was
22 replaced by dry-etching using plasma. Gao et al. ^[50] used black silicon instead of the
23 conventional pSi. The relationship between black silicon morphology and its NIMS sensitivity
24 was studied using several biomolecules: spermidine, arginine, adenosine, palmitoyl carnitine,
25 verapamil, bradykinin, and STAL-2. It was found that the black silicon pillars absorb enough
26 initiator promoting desorption of analytes, and that large surface areas can efficiently improve

1 NIMS sensitivity due to the enhanced energy transfer from substrates to analytes. The same
2 dry-etching method was used to create an integrated microfluidics-NIMS device.^[52] In this
3
4 investigation, the novel NIMS substrate is compatible with droplet and digital microfluidics
5
6 and can be used on-chip to assay glycoside hydrolase enzyme in vitro.
7
8
9

10 11 *2.1.3. Functionalization with metals*

12 Alternative studies presented the use of metals to functionalize the pSi surface. Zhou et al.^[40]
13
14 used several chemical reactions to obtain phosphonate-terminated pSi which was immersed into
15
16 ZrOCl₂ solution to yield the Zirconium Phosphonate-Modified Porous Silicon (ZrP-pSi) wafers.
17
18 The obtained ZrP-pSi wafers were sensitive to phosphopeptide detection and their high
19
20 specificity was demonstrated by the analysis of tryptic digest product of α -casein, β -casein and
21
22 BSA. Latest research specifically focused on the use of silver as surface functionalizing agent
23
24 for pSi. Yan et al.^[41] used different mixtures of silver nitrate in water, 4-ATP in ethanol and
25
26 trifluoroacetic acid (TFA) to prepare substrates with and without well-organized 4-ATP self-
27
28 assembled monolayers. The study demonstrated that the 4-ATP capped substrate was more
29
30 efficient than the substrate covered by naked Ag nanoparticles exhibiting higher ionization
31
32 efficiency and less fragmentation. The substrate performance was excellent, with limits of
33
34 detection down to several femtomoles for TPyP, sub picomoles for oxytocin, and picomoles for
35
36 PEG 400 and PEG 2300. A different approach to obtain silver covered pSi was described by
37
38 Gustafsson et al.^[42] The DIOS substrates were prepared by electrochemical etching and
39
40 immediately sputter-coated with a 1.4nm-thick Ag layer. For testing, this new DIOS/Ag-DIOS
41
42 MSI method, distributions for fingerprint compounds and tissue metabolites of 6-bromoisatin
43
44 were mapped. Fingerprint analysis showed a broad range of small molecule classes, including
45
46 environmental contaminants (ditallow dimethyl ammonium chloride, DTDMAC), lipids (FAs,
47
48 TAGs), sterols and wax esters (WEs). The imprinted murine fore-stomach tissue analysis
49
50 showed phosphatidylcholine head group (PC), 6,6'-dibromoindirubin (6,6'-DBI), fatty acids
51
52
53
54
55
56
57
58
59
60
61

1 (FAs), cholesterol and Ag cluster peaks. This novel approach exhibited minimal observable
2 depletion and has the potential to simplify the analysis of multiple compound classes by using
3 a single analytical platform to acquire multi-tiered spatial data sets. Gold was also used to
4 functionalize pSi by Li et al.^[46] They used electrochemical deposition method to obtain a new
5 pSi chip functionalized with gold nanoparticles (PSi-GNPs) that allows direct serum peptide
6 profiling with a high-quality MS signal. Using both silver and gold nanoparticles is also
7 possible; Wang et al.^[47] created patterned nanoporous silicon chips embedded with Ag and Au
8 NPs by chemical assisted etching for detection of thiol compounds. In this case, the selectivity
9 of the Ag and Au NPs embedded chips towards thiol compounds was monitored in cells. Also,
10 the effect of irinotecan, 7-ethyl-10-[4-(1-piperidino)-1-piperidino]-carbonyloxy camptothecin
11 (CPT-11), which is a potent anticancer drug, was determined using the novel chips.
12
13
14
15
16
17
18
19
20
21
22
23
24
25
26
27
28

29 *2.1.4. Other functionalization methods*

30 For specific applications that characterize bio-systems, functionalization of pSi implies the
31 formation of particular Si- bonds on the surface of pSi. This method was used to enhance
32 detection of slightly larger molecules such as peptides or proteins, together with the use of an
33 organic matrix. Several research groups^[27,28,34] developed such analytical methods. Chen et al.
34^[27] analyzed a specific protein system, NTA-Ni²⁺/His-tagged protein, with carboxyl (–COOH)
35 functionalized pSi microarray. The groups of Chen et al.^[34] and Yan et al.^[28] have immobilized
36 antibodies on the pSi surface by physical adsorption. These experiments resulted in the
37 detection of biomarker B-type natriuretic peptide (BNP) with a detection limit as low as
38 10pg/mL BNP in human plasma^[34] and the specific detection of angiotensin I at a 10 fmol level
39 in diluted plasma samples (10 μ L, 1 nM).^[28] Another specific biological system characterization
40 method was developed by Sweetman et al.^[45] where the attachment of mammalian cells to pSi
41 was studied. For this, NHS ester and PEG-functionalized pSi surfaces were conjugated with
42
43
44
45
46
47
48
49
50
51
52
53
54
55
56
57
58
59
60
61
62
63
64
65

1 adhesion mediator protein fibronectin (FN) and used for the selective immobilization of human
2 neuroblastoma cell line SK-N-SH.
3
4
5
6

7 **3. Silicon nanostructures: nanoparticles, nanowires, and nanostructured surfaces**

8
9 Nanostructures such as nanoparticles (NPs), nanowires (NWs), nano-flowers, nano-pillars etc.,
10 have been well studied for their applications in the biomedical area. Lately, silicon and silica-
11 containing NPs, silicon NWs and nanostructured silicon surfaces were demonstrated to be
12 useful substrates for MS analysis of several types of biomolecules including small drug
13 molecules, peptides, proteins, lipids, immobilized DNA. The mass spectrometry techniques
14 using these substrates are known as surface-assisted laser desorption/ionization mass
15 spectrometry (SALDI-MS) and nanostructure assisted laser desorption ionization mass
16 spectrometry (NALDI-MS).^[13] As for pSi, silicon nanostructures can be used together with
17 organic matrices for detecting larger molecules.
18
19
20
21
22
23
24
25
26
27
28
29
30

31 In this section, several nanostructured substrates will be described based on their synthesis
32 method, functionalization method and use in LDI-MS analysis. The fabrication methods will
33 be divided into three categories: nanoparticles and nano-powders (3.1.1), nanowires (3.1.2) and
34 nanostructured surfaces (3.1.3). **Table 2** shows a resume of the several substrates, according to
35 their fabrication method and target application. The surface modification methods will be
36 divided into three categories: derivatization using silylating reagents (3.2.1), functionalization
37 with metals (3.2.2) and finally, other functionalization methods (3.2.3).
38
39
40
41
42
43
44
45
46
47
48
49
50

51 **3.1. Fabrication methods**

52 *3.1.1. Silicon/silica nanoparticles*

53 Silicon and silica-containing nanoparticles have emerged as a reliable alternative to organic
54 matrices for LDI ever since pSi demonstrated its extensive value in MS applications. As a result,
55 many groups developed a variety of silica and silicon nanostructures. Silica nanoparticles can
56
57
58
59
60
61
62
63
64
65

1
2
3
4
5
6
7
8
9
10
11
12
13
14
15
16
17
18
19
20
21
22
23
24
25
26
27
28
29
30
31
32
33
34
35
36
37
38
39
40
41
42
43
44
45
46
47
48
49
50
51
52
53
54
55
56
57
58
59
60
61
62
63
64
65

be easily synthesized by wet chemical methods but they are available to be purchased from several commercial distributors as well. Dupre et al. chose to prepare SiO₂ nanoparticles through the very well-known sol-gel method. The group used a solution of ammonium hydroxide in methanol and tetraethoxysilane (TEOS) as the precursor for the silica NPs. After all the necessary steps were completed, the SiO₂ NPs were dried at room temperature.^[55] Following the example of SiO₂ NPs, core-shell nanoparticles (CSNPs) have also been used as matrix-free substrates for LDI-MS experiments. These nanostructures proved to be more complex and in need of a rigorous design for each application. The synthesis of such nanoparticles was carried out mainly using sol-gel processes. For example, magnetite core-shell particles were prepared by several groups ^[56-59], where the core was a magnetite nanoparticle and the shell was a thin silica layer. Briefly, the CSNPs were synthesized by coating the magnetite particles with a thin silica layer through the sol-gel process with TEOS as the silica source. Xiong et al.^[59] designed and synthesized aptamer-immobilized magnetic mesoporous silica/Au nanocomposites (MMANs) (**Figure 2**) for highly selective detection of unlabeled insulin in complex biological media using MALDI-TOF MS (with CHCA matrix). Briefly, the aptamer was anchored onto the gold nanoparticles in the mesochannels of MMANs for efficient and specific enrichment of insulin. Zhu et al. approached the CSNP method differently. The magnetite core was substituted by AuNPs (between 18 and 50 nm) and the outer layer was an ultrathin silica shell (~2-4 nm). The adhesion between gold and silica was possible due to the prior functionalization of the AuNPs' surface with amino groups.^[60] However, other groups ^[61-63] chose to purchase the SiNPs and experimented with storage and functionalization methods.

3.1.2. Silicon nanowires

Silicon nanowires (SiNWs) used in LDI-MS experiments have been primarily synthesized using vapor-liquid-solid (VLS) growth mechanism.^[64-66] The VLS method uses a nano-sized catalyst metal (deposited onto the silicon wafer) that can rapidly adsorb gaseous precursors

1 from which the growth of nanowires occurs. The growth and diameter of SiNWs are directly
2 dependent on the Au colloid particles' size. In this case, the groups that developed SiNWs have
3
4 used Au nanocluster catalyzed VLS growth mechanism. Briefly, Au nanoparticles are
5 distributed on a silicon substrate by spin-coating, then solvents and organic residues are
6 removed and finally the growth of SiNWs is obtained during chemical vapor deposition with
7 silane as the vapor-phase reactant. Muck et al. [66] combined the VLS growth method with the
8 typical fabrication methods of patterned silicon: photolithography, wet-chemical etching, and
9 dry plasma etching. Firstly, the silicon substrates were patterned with holes (~50 nm depth)
10 arranged in arrays of 2.5 μm circles with a 4.5 μm pitch (**Figure 3**). Lastly, the patterned
11 silicon served as the substrate where the SiNWs were grown at the bottom of the etched holes
12 by the VLS method using chemical vapor deposition from silane. SiNWs were commercially
13 available for a limited time from Bruker.^[80]

31 3.1.3. Nanostructured silicon surfaces

32 Along with the use of silicon nanoparticles and nanowires, silicon nanostructured surfaces have
33 also been tested as LDI-MS substrates.^[67-77,79,80] In most of the studies, the nanostructured
34 surfaces are referred to as silicon nanowire arrays. These are densely packed arrays of vertical
35 nanopillars, also called black silicon (BSi), not to be confused with silicon nanowires. The
36 fabrication methods of these substrates can be categorized in two: wet etching and dry etching.
37 The most popular fabrication method for silicon nanowire arrays is chemical etching (see
38 **Figure 4**).^[67-70] Briefly, Si wafers are cleaned using well-known methods (Piranha solution,
39 sonicating in acetone, isopropanol, methanol, rinsing with deionized water, etc.) to obtain clean
40 and oxide-free Si surfaces, then the wafers are etched in a solution of $\text{AgNO}_3/\text{H}_2\text{O}/\text{HF}$ of
41 different concentrations to form bare silicon nanopillars. This classical method was slightly
42 modified and replaced by metal-assisted chemical etching (MACE).^[71-74] In this case, a new
43 step is added to the process. After Si wafer cleaning, a thin layer of Au is deposited onto Si
44
45
46
47
48
49
50
51
52
53
54
55
56
57
58
59
60
61
62
63
64
65

1 substrates and then immersed in an HF/H₂O₂/EtOH etching mixture to create nanostructured
2 silicon on the wafer.
3

4 However, all chemical etching methods use very toxic and dangerous substances for the user.
5

6 For example, the piranha solution is a mixture of H₂SO₄/H₂O₂, which is a strong oxidant that
7 reacts violently with organic materials and can cause severe skin burns. Another dangerous
8 substance used is HF, which is a hazardous acid that can cause serious tissue damage if burns
9 are not appropriately treated. All etching processes must be handled with extreme care in a well-
10 ventilated fume hood while wearing appropriate chemical safety protection: face shield, double
11 layered nitrile gloves, etc.^[61,67,71] All these factors can reduce the interest of groups in using
12 these methods.
13
14
15
16
17
18
19
20
21
22

23 Alternative solutions, consisting of variations on dry etching methods used in creating
24 nanostructures on silicon wafers have quickly emerged.^[75-79] Basically, the silicon wafers are
25 etched using plasma in the presence of a protective mask. In the work of Gulbakan et al.^[75] an
26 alumina mask was used together with argon plasma with various etching parameters to form
27 different pore depth nanowell arrays. In the work of Wang et al.^[76], the mask was a polystyrene
28 (PS) nanosphere monolayer and the plasma was formed by a mixture of etching gases: SF₆,
29 CHF₃, and O₂. In this case, the resulting nanostructure was a biomimetic silicon nanocone array,
30 with cone heights ranging between 200-600 nm. Morris et al. used traditional microelectronic
31 fabrication steps for all the process: first they patterned the silicon wafer using deep-UV-
32 photolithography technique and after they performed silicon etching using both ICP and RIE
33 and a mixture of etchant gases: C₄F₈, SF₆, and Ar. This resulted in well-ordered silicon nanopost
34 surfaces (NAPA) that were useful for small molecule analysis (Figure 4).^[77,78] The fabrication
35 method of Chen et al.^[79] is slightly unconventional compared to the above-presented techniques.
36 The silicon wafers were exposed to repeated laser irradiations in the presence of air, SF₆ gas or
37 deionized water. This method however generated mostly microcolumn arrays but with special
38
39
40
41
42
43
44
45
46
47
48
49
50
51
52
53
54
55
56
57
58
59
60
61
62
63
64
65

1 conditions (600 laser shots at 0.13 J/cm^2 in water environment) submicrometer microcolumns
2 were generated with average 800 nm height and periodicity 600 nm.
3
4
5
6

7 **3.2. Nanostructure derivatization and functionalization methods**

8 All dry techniques presented in this review produced stable substrates without additional
9 modifications, contrary to the surfaces produced by chemical attack. The latter were stabilized
10 during derivatization or functionalization. All methods are summarized in **Table 2** below.
11
12
13
14
15
16
17

18 *3.2.1. Derivatization using silylating reagents*

19 The groups in ^[61,62] chose to silylate purchased SiO_2 nanoparticles with PFP, PHP, TMS, C10,
20 C6, and C3, and test the silicon-nanoparticle-assisted laser desorption/ionization (SPALDI)
21 method on pharmaceuticals, peptides, pesticides, nucleic acids, and salt derivatives. The SiNPs
22 were oxidized with HNO_3 before silylation, and after silylation they were mixed with the
23 analyte solutions and spotted on standard MALDI plates. Nanowires have also been silylated
24 with PFPPDCS.^[64,65] In both cases the SiNWs were first etched in HF solution to remove the
25 oxide layer and then reoxidized with ozone, followed by the final silylation step. Go et al. ^[64]
26 examined the effect of laser energy, nanowire density, nanowire size, and growth orientation of
27 the SiNWs while performing mass spectrometry experiments on peptides and small drug
28 molecules. Luo et al. focused on studying the internal energy transfer in SALDI from SiNWs
29 and its relationship to nanoporous silicon in DIOS and to conventional MALDI.^[65] By means
30 of benzyl-substituted benzylpyridinium thermometer ions, the authors in ^[65] could prove that
31 very low laser fluence is needed for LDI, due to the high thermal energy confinement achieved
32 in SiNWs. The chemically etched substrates ^[67–69] were modified with OTS, FDTS or ODCS.
33 These studies were mostly focused on validating the use of the new substrates by detection of
34 various types of peptides and small molecules. Lastly, a silylated (with F_{13}) MACE substrate
35 was used to detect peptides (middle range 1–3 kDa) and methadone (low range <500 Da). ^[72]
36
37
38
39
40
41
42
43
44
45
46
47
48
49
50
51
52
53
54
55
56
57
58
59
60
61
62
63
64
65

The substrate allowed for the detection of methadone in saliva, blood plasma and urine from clinical samples of real methadone-treated patients.

3.2.2. Functionalization with metals

Metallic nanoparticles such as gold and silver have previously demonstrated their efficiency in MS experiments^[3,81], so functionalizing nanostructures substrates with metals is a compelling opportunity for enhancing LDI substrates. Au was used by various groups as a functionalization agent^[59,63,73]. Xiong et al.^[59] modified magnetite core-shell nanoparticles with Au NPs on the silica outer shell obtaining aptamer-immobilized magnetic mesoporous silica/Au nanocomposites (MMANs). The main use of these composite nanoparticles is for insulin detection, however, more proteins were detected as well: immunoglobulin G, human serum albumin, α 1-antitrypsin, horseradish peroxidase, lysozyme, and cytochrome C. Another group^[63], attached purchased silica nanoparticles to a silicon wafer using polymers for adhesion. Then the SiNPs were modified with Au by immersion of the wafer into an AuNP solution. This way the AuNPs constructed the outer layer of the substrate facilitating the formation of a self-assembled monolayer (SAM) of Capture DNA-1. The final substrate was an Au and SiO₂ NPs-assembled hybrid porous nanostructure and was used to analyze confined DNA structures. Another method to create AuNPs on nanostructured surfaces was developed by Tsao et al.^[73] The nanostructured Si surface was oxidized with O₂ plasma and immersed in HF/HAuCl₄ solution to graft the Au nanoparticles. The resulting AuNPs-nSi chip was used as LDI-MS substrate for the analysis of glucose from standard solutions and urine. High detection sensitivity and specificity for glucose in a biological sample confirmed the potential of the substrate.

Other metals used to create functional substrates were Cu^[57], Li^[66], and Ag^[70]. Copper was used for the surface grafting of magnetite core-shell nanoparticles with Cu²⁺ ions. The functional microspheres could capture small peptides from complex sample systems (human

1 serum and urine) with the large proteins excluded because of the porosity of mesoporous silica
2 and the specific affinity of Cu^{2+} ions toward peptides.^[57] Muck et al. chose Li as a doping agent.
3
4 In this case, the sample solutions were deposited on the silicon nanowire substrate and the
5
6 $^7\text{LiOH}$ solution was deposited after the sample dried. The $^7\text{LiOH}$ solution was prepared in
7
8 methanol–dichloromethane 1:4 at 7.5 mg mL^{-1} . Most of the compounds were detected as clean
9
10 $[\text{M}+^7\text{Li}]^+$ signals.^[66] Finally, AgNPs were used to decorate silicon nanowire arrays by a pulsed
11
12 laser deposition method.^[70] The applicability of AgNP-decorated SiNWs was demonstrated by
13
14 the detection of unsaturated compounds (SQ and oleic acid) in a complex matrix.
15
16
17
18
19
20
21

22 3.2.3. Other functionalization methods

23 Some groups chose to approach the functionalization method differently. The study by Chen et
24
25 al.^[56] modified the surface of magnetite core-shell nanoparticles (CSNPs) first by modification
26
27 with MPS and finally by a seeded aqueous-phase radical polymerization with MMA. These
28
29 CSNPs were specifically designed for the enrichment of peptides and proteins for mass
30
31 spectrometric analysis. Other groups have also designed their novel substrate based on
32
33 magnetite CSNPs roughly for the same purpose: selective enrichment of peptides.^[58] In this
34
35 case, the microspheres were dried and calcined in nitrogen to improve the hydrophobic property
36
37 of the surface. A different study developed CSNPs with AuNP core and ultra-thin silica shell.^[60]
38
39 The stabilization of these Au@utSiO₂ CSNPs was carried out by further growth of the silica
40
41 shell using the Stöber method. Small functional molecules and small polymers were
42
43 successfully detected by CSNP-based LDI-TOF-MS. In 2008 Daniels et al.^[80] functionalized
44
45 commercially available NALDI target plates from Bruker Daltonics, Billerica, MA. The surface
46
47 of the silicon nanowires was modified by depositing organic layers to change the
48
49 hydrophobicity of the substrate. The new target plate was used for the detection of small
50
51 molecules. Unfortunately, there is no mention about the organic layer type and the NALDI
52
53 plates are no longer available for purchase.
54
55
56
57
58
59
60
61

4. LDI mechanism: ionization and desorption processes

Matrix-assisted laser desorption/ionization mass spectrometry (MALDI-MS) has become an indispensable analysis technique for many research communities since its first use by Karas et al. in the 80s.^[82] The fundamental strategy of a complete MALDI-MS analysis consists of several steps: sample preparation, excitation of sample and desorption of the condensed phase, ionization of analyte molecules by the generation of charges, extraction, and detection of ions.^[83] The processes that occur between the excitation of the sample and the extraction of ions are collectively called laser desorption/ionization (LDI) mechanism. This mechanism is most commonly considered as a convolution of two processes: desorption and ion formation. These processes have been previously studied in detail by several groups.^[83–87] LDI is portrayed as a complex process that involves both optical and mechanical phenomena as well as thermodynamic and physicochemical processes of phase transition and ionization. Ionization, in particular, was described as a collection of chemical and physical pathways including gas-phase photoionization, ion-molecule reactions, disproportionation, excited-state proton transfer, energy pooling, thermal ionization, and desorption of preformed ions.^[84] The LDI mechanism has been an active topic of research and was revisited by Chang et al. and Jaskolla et al.^[86,87] Since the first years of MALDI analysis, ionization of analytes was helped by an organic matrix that possesses some essential functions. First, it has to isolate analyte molecules by preventing analyte aggregation. Then, it has to absorb the laser energy while the disintegration of the condensed phase takes place without excessive destructive heating of the analyte molecules. Lastly, the matrix should provide an efficient ionization of analyte molecules.^[84] With all these specificities of the matrices, however, the generated spectra are far from ideal and the use of a matrix is not as suitable for untargeted MS experiments focused in small molecules. The matrix complicates the sample preparation, introduces background ions in the spectra, hampers quantitative analysis and also complicates the acquisition of MS images at high lateral resolutions. These difficulties may be reduced by replacing the organic matrix with a less

invasive component that has at least the same specific/required properties as the matrix.

Therefore, by understanding the LDI mechanism of molecules adsorbed to a specific substrate, especially nanostructured silicon, one could be able to maximize ion yields, control analyte charge states and fragmentation, and gain access to analyzing new classes of compounds.

This section provides an overview of the LDI mechanisms described in LDI-MS experiments using silicon-based substrates instead of organic matrices. The specific physicochemical properties of the substrate necessary for aiding desorption and ion formation will be discussed, as well as the specific LDI processes for each substrate type.

4.1. Influence of physical properties

4.1.1. Porous silicon

For pSi, the main influencing factors of the LDI process are considered to be the physical properties of the material surface. The pSi structure has a high surface area which provides an optimal environment for the co-adsorption or entrapment of the analyte and solvent.^[23,24,29,53] High pore density and smaller pore sizes might produce better results as the increase in ion signal can be correlated with the increase of the overall surface area and analyte coverage. Furthermore, the tendency of energy localization near defects, protrusions, and edge sites makes these areas more active in LDI processes.^[23,53] In addition, analyte penetration into the pSi is critical because the pSi also manifests quantum confinement effects: large optical absorption and low thermal conductivity. These effects cause rapid heating of pSi in the presence of laser and the resulted energy may be transferred from silicon to the trapped analyte. Basically, instant heating of the pSi provides the necessary energy for analyte desorption and ionization.^[23,29]

4.1.2. Nanostructured silicon

Silicon nanostructures such as nanoparticles, nanowires, and nanostructured surfaces have specific physical properties that favor LDI processes. Although many different nanostructures have been fabricated, their properties are common for most of them: specific dimensions that

1 maximize laser light absorption, specific heat capacity and conductivity of the nanostructured
2 silicon and geometric effects that promote molecule adhesion and desorption.
3

4 For silicon nanowires, the main features correlated with efficient LDI are morphology and low
5 thermal conductivity. For example, the ionization performance of nanowires was described as
6 strongly dependent on wire length and density.^[64] Here, SiNWs act as tiny antennas where the
7 laser energy is efficiently absorbed. When the energy is focused on a small area it generates a
8 field desorption effect resulting in the gas-phase generation of the deposited analyte molecules.
9 This energy focusing effect primarily promotes desorption of molecules and results in very little
10 surface-related background ions.^[64] The SiNW arrays showed superior laser desorption
11 properties by requiring lower laser energy to desorb molecules.^[66] In this case, the obtained
12 signal was enhanced due to three main reasons. Firstly, because of the increased absorption of
13 the nanowire forest near the wavelength of the laser, then because of the fast heating of the
14 silicon core within the insulating oxide sheath and lastly because of the large surface area of
15 the nanostructures.^[66] The group of Vertes et al. ^[65] has committed to thoroughly study the
16 internal energy transfer in laser desorption/ionization from silicon nanowires. They also refer
17 to geometry and thermal properties of the SiNWs as main influencing factors on the more
18 efficient energy transfer resulting in a more efficient desorption.
19
20
21
22
23
24
25
26
27
28
29
30
31
32
33
34
35
36
37
38
39
40

41 In the case of nanostructured silicon surfaces, the key physical factors that promote efficient
42 ionization are the structure's morphology and its optical and thermal properties. For example,
43 the dimensions of the nanostructured silicon surfaces described by several groups ^[70,72,76,77]
44 were directly associated with ionization efficiency. In these cases the ion intensity decreased
45 considerably with length increase, the longer structures (> 450 nm ^[72]) did not allow efficient
46 energy transfer from the laser to the analyte. Morris et al. ^[77] correlated three main features of
47 their nanopost arrays with optimum LDI, namely: (1) well-ordered nanopost arrays, (2)
48 dimensions that maximize laser light absorption and subsequent resonance effects that promote
49 analyte desorption and ionization, and (3) a highly porous surface to maximize analytical
50
51
52
53
54
55
56
57
58
59
60
61
62
63
64
65

1 sensitivity. Gulbakan et al. [75] have also suggested that these factors generate a local
2 environment to which analytes adhere with optimal heat capacity and heat conductivity that
3
4 result in effective absorption of laser light followed by effective sublimation.
5
6

7 Another morphological aspect that was associated with increased ionization efficiency was
8
9 surface roughness. It was implied that the surface roughness has a more direct effect on the ion
10
11 intensity efficiency than the silicon nanostructure pore size, depth and surface area/volume
12
13 ratio.^[71]
14
15
16
17
18

19 **4.2. Influence of functional group**

20 *4.2.1. Porous silicon*

21 Another factor that affects the LDI mechanism of pSi is the chemical property of the surface.
22
23 Hydrophobic or hydrophilic groups may cover the substrate surface and affect the analyte
24
25 adsorption on the pSi. Hydrophobic surfaces may give intense MS signals for hydrophobic
26
27 analytes from aqueous medium because the solvent is not confined to the porous area.^[23] On
28
29 the contrary, hydrophilic surfaces enhance adsorption of all molecules from an aqueous medium
30
31 onto the pSi and result in lower ion desorption efficiency.^[44] In the case of derivatized substrates
32
33 with terminal hydride and silanol groups, deposition of the analyte leads to the adsorption and
34
35 trapping of the solvent.^[53] Another example is the interaction between the analyte and metallic
36
37 cations. Ag is a well-known cationization agent that produces enhanced D/I processes.^[42] LDI
38
39 of analyte molecules using Ag nanoparticles is obtained through high absorption and low
40
41 reflection of energy. The laser energy is quickly absorbed by the Ag nanoparticles which are
42
43 rapidly heated, resulting in the vaporization and ionization of the analyte molecules.^[41] In the
44
45 same study, the surface was functionalized with 4-ATP as well, which acted as a matrix. This
46
47 small aromatic molecule enhanced the absorption of energy in the ultraviolet region. Gold is
48
49 another well-known metal used to functionalize pSi surfaces for enhanced ionization.^[46,47] Li
50
51 et al. [46] describe the effect on ionization of the plasmonic property of AuNPs. They assume
52
53 that AuNPs may act primarily as antennae which concentrate the laser-induced field within the
54
55
56
57
58
59
60
61
62
63
64
65

nanoporous channel, which leads to an enhanced MS signal. They also postulate that plasmonic metals absorb resonant photons, and the energetic electrons formed by the SPR excitation are transferred to the semiconductor (Si), leading to the accumulation of positive charges on the metal surface.

4.2.2. Nanostructured silicon

Chemically derivatized silicon nanostructures have been designed and synthesized to improve the LDI efficiency mainly by separating targeted molecules from biological media and inducing a controlled ionization of the selected analytes. In case of the group of Liu et al.^[57], this process consists in functionalizing the magnetic mesoporous microspheres with immobilized Cu²⁺ for a high efficiency in peptide enrichment. Another example is for the aptamer functionalized magnetic nanoparticles. These were used to enhance the MS intensity of insulin, where aptamer and magnetism facilitate immunoreactions between the aptamer and the target, improving detection sensitivity.^[59]

A more traditional chemical improvement of nanostructured silicon was reported by Morris et al.^[77] In this study, the silanol groups are used as proton source for ionization and to induce increased analyte sensitivity. They described the presence and electronegativity of fluorine as a factor that increased the acidity of the silanol group, thus providing a favorable environment for the protonation of molecules. The altered chemical composition of the silicon nanostructures also affects optical absorption. In the case of Chen et al. the absorption values of microcolumns are increased across the entire UV-visible spectrum, and significant absorption extends into the near-IR region.^[79]

4.3. Influence of other interactions

4.3.1. Porous silicon

Proton affinity of certain analytes has been also speculated to affect ionization.^[33,44,53] The ionization efficiency is similar for analytes with comparable secondary amino groups (e.g.

1 structurally related MA and MDMA) while the ionization efficiency is higher for other analytes
2 (e.g. cocaine), which contain tertiary amino groups, that have higher proton affinity.^[33]
3
4 Functional groups and solvents are the primary proton sources, so the right combination
5
6 between the substrate, the analyte, and the solvent could be critical for optimal DIOS efficiency.
7
8 External elements, such as laser fluence and substrate storage, impact the D/I process as well.
9
10 High laser fluence results in analyte fragmentations that could lead to crowded mass spectra in
11
12 the low mass range. This is sheer evidence of the thermal driving force in the D/I process.
13
14
15
16
17
18

19 4.3.2. Nanostructured silicon

20 Some LDI mechanisms are not directly affected by the physicochemical properties of the
21
22 substrate but by the inherent physicochemical properties of analytes such as pI (isoelectric
23
24 point), hydrophobicity, hydrophilicity, number of charges and their concentration. For example,
25
26 due to each molecule's specific pI and due to the sample pH, some molecules appear as
27
28 negatively charged ions and cannot be detected in positive mode and vice versa. One example
29
30 of negatively charged molecule is fibrinopeptide B, due to the presence of three glutamic acid
31
32 and one aspartic acid residues in its sequence.^[68] In this study, the super-hydrophilic pattern of
33
34 the surface was investigated as well. This specific surface promoted a better ionization
35
36 efficiency of peptides because most peptides are positively charged and adsorb specifically to
37
38 the SiO₂ surface. This specific adhesion property of biological samples has been attributed to
39
40 amino acid residues that have different adhesion properties to inorganic interfaces such as SiO₂,
41
42 Si₃N₄, and metals, essentially depending on their side chains.^[68]
43
44
45
46
47
48

49 Other external factors that affect the LDI mechanism are laser energy and laser plume. So far
50
51 laser energy has been discussed as UV light efficiently absorbed by the silicon nanostructures.
52
53 Laser energy can be varied to induce different effects on the D/I processes. Zenobi and
54
55 Knochenmuss^[84] described in great detail ion formation and the effect of laser fluency in the
56
57 classical MALDI process. A similar description could be given for nanostructure assisted LDI.
58
59
60
61
62
63
64
65

1 However, several authors imply that the optimal laser intensity required to get good MS signals
2 is typically much lower than that required for both standard MALDI and DIOS.^[88-90] This is
3
4 assumed to be due to the optical and thermal properties of silicon nanostructures. The low laser
5
6 fluencies are also beneficial in the ionization of thermally labile compounds because it may
7
8 reduce the necessary energy for desorption and it may also reduce fragmentation.^[79]
9

10
11 The laser plume effect has been described as the presence of electrons in the laser plume due to
12
13 photoelectric effects. Ions can be generated through electron impact ionization or recombination
14
15 between electrons emitted from the plume and analyte surface. This way the desorbed species
16
17 mix with the plume and after ion-molecule reactions protonated species are generated. At
18
19 increased laser power, the elevated electron density can neutralize the protons to form
20
21 hydrogen-free radicals, meanwhile, more alkali ions are released from the hot silicon surface
22
23 that results in peptide-alkali adduct ion formation.^[79]
24
25
26
27

28
29 Another interesting hypothesis suggested that absorbed UV laser energy was transferred from
30
31 the surface to pre-charged analytes causing desorption.^[79] However, it is unclear whether the
32
33 protonation process happens in solution (before laser interaction) or it is a laser-induced proton
34
35 transfer on/near the surface. Also, residual solvents retained in the cavities of the nanostructured
36
37 surfaces are probable sources of protons that help to ionize analytes.^[79] Tsao et al. proposed
38
39 another ionization process: glucose samples were catalyzed to negatively charged gluconic acid
40
41 molecules by the on-chip AuNPs-nSi surface Au- based catalyst reactions.^[73] In this case,
42
43 enhanced detection sensitivity was a result of the Au nanoparticles grafted to the nanostructured
44
45 silicon surface.
46
47
48
49

50 51 52 **5. Discussion**

53 Silicon is one of the prime candidates for fabrication of LDI-MS substrates for three main
54
55 reasons: silicon is biologically inert; the silicon technology is very advanced and flexible, and
56
57 silicon nanostructures can be designed with controllable morphology and properties for LDI-
58
59

1 MS. It is important to mention that silicon is a material that can be easily stabilized, derivatized
2 and functionalized.
3

4 In case of silicon substrates designed for LDI-MS experiments, the wet (chemical) fabrication
5 techniques used to create pSi slowly evolved to dry (physical) techniques. Wet techniques use
6 highly toxic compounds (ex.: piranha solution for cleaning and HF for etching) for dangerous
7 fabrication methods (ex.: electrochemical etching in a closed Teflon cell). Therefore, dry
8 fabrication techniques have emerged that eliminate all dangers to the user. These techniques
9 also improve the essential needs of a good quality substrate: fabrication process is highly
10 repetitive, the surface is free of air or liquid contaminants, automated fabrication is possible and
11 most importantly, no danger for the user. Most of the dry fabrication techniques are derived
12 from the micro/nanoelectronics fabrication methods. This is another reason why dry fabrication
13 methods are becoming more popular: silicon technology is improving day by day and together
14 with it, silicon nanostructure fabrication methods keep advancing.
15
16
17
18
19
20
21
22
23
24
25
26
27
28
29
30

31 Silicon nanostructures of all types: nanoparticles, nanowires, black silicon, pSi, etc., have been
32 stabilized and derivatized using different strategies for many purposes. There is no standard
33 procedure for all types of experiments. Muthu et al. ^[89] suggested that the sample preparation
34 is an art form, and, given its complexity, surface modification of any silicon nanostructure can
35 also be considered an art form. Surfaces can be modified with a variety of agents: from metallic
36 nanoparticles (Ag, Au, Cu, etc.) to small (amine groups, perfluorophenyls, etc.) and big (neat
37 silane, antibodies, etc.) biomolecules (Table 1 and 2). Depending on the application of the
38 substrate, one can design a targeted analysis method by choosing the appropriate
39 functionalization method and/or combine various functionalization methods to reduce
40 unwanted signal or to obtain a broader range of detection. It all depends on the users' creativity.
41
42
43
44
45
46
47
48
49
50
51
52
53
54
55
56
57
58
59
60
61
62
63
64
65

All these surface-modified matrix-free methods can be used together with an organic matrix to
expand the detection range from small to large molecules.

1 Although silicon nanostructures can be very repetitive and homogeneous, the reliability of the
2 LDI-MS measurements depends also on the sample deposition method. Irreproducible sample
3 deposition leads to irreproducible results. This is strongly related to the uneven crystallization
4 of liquid samples on the substrate which induces signal variation between different spots of the
5 same sample. For this reason, sample deposition was rigorously studied for silicon
6 nanostructures. In the case of pSi, reproducible liquid sample deposition was achieved through
7 acoustic printing.^[50,91]

8 As we have described above, silicon-based nanoparticles/nanowires have been used as LDI
9 substrates. In this case, the sample analyte is usually mixed with the nanoparticle/nanowire
10 solution in the appropriate concentrations prior to spotting on the MALDI target plate and
11 subsequent co-crystallization.^[60,61] Although this wet chemistry deposition technique is very
12 flexible, it suffers from the same problems as in the case of the organic matrices (i.e.
13 heterogeneous spots).

14 Most of the studies mentioned in this report focus on liquid samples, however, the analysis of
15 tissues is highly demanded as well. The first issue to be considered in an MSI experiment is the
16 performance of the substrate-tissue-air system. In current standard MALDI analysis, the tissue
17 is cut into ~10 μm thick slices and each slice is mounted onto an indium tin oxide (ITO) coated
18 glass slide, then coated with a thin layer of matrix.^[8] In this case, the thickness of the tissue
19 does not affect the transfer of energy from the laser to the matrix and implicitly the tissue for
20 LDI processes. In other cases, when the matrix and the ITO glass slide are replaced by a
21 nanostructured surface on which the tissue is mounted, the thickness of the tissue matters. The
22 laser energy has to pass the tissue and reach the nanostructured surface in order to promote the
23 ion desorption and ionization processes. In NIMS applications, in order to facilitate the laser to
24 get to the tissue-nanostructure interface, the tissue slices are 3-5 μm thick, so they are much
25 thinner than in usual MSI experiments.^[43,48,49] Even in this case, a high laser power is needed
26 which mostly results in burning the tissue and produces harder ionization. Moreover, NIMS

MSI experiments have not been reported on Bruker MALDI-MS spectrometers, which suggests that there is some instrumental limitation with this manufacturer.

An alternative technique that avoids the effect of tissue thickness, consists of imprinting (or stamping) a tissue over the surface.^[36] The imprinting process consists in putting the tissue in contact with the nanostructured substrate and then removing it, leaving only the adhered molecules from the tissue sample onto the substrate. Although it avoids the cutting of thin tissue samples and depositing them over the surface, the imprinting processes have been reported to lack reliability because of possible smears.^[92] Within this method, new applications of MSI in the clinical practice are envisaged, consisting in the imprint of a tissue on a silicon-based substrate for needle biopsy processes, without the need to remove the biopsy tissue.^[93]

The imprinting process is compatible with the new strategies developed to create specific adhesion of molecules to the nanostructured surface through surface functionalization. The silicon-based nanoparticle methods presented in this review often use linker molecules for specific detection of analytes. This approach should be considered for nanostructured silicon surfaces as well.

Guidelines for detecting biomolecules by Si LDI-MS

All detected molecules and detection strategies used in the publications presented in this progress report are listed in **Table S3** and summarized in **Figure 5**. The bar charts in **Figure 5** show the great versatility of Si based substrates, as all types of Si substrates have been used to detect most types of biomolecules. Since there are no standard protocols for detecting all kinds of molecules simultaneously, each strategy is focused on detecting specific biomolecules. As such, we highlight the following trends in Si LDI-MS:

- A. Peptides and proteins are often detected with the help of organic matrices while small molecules do not need the organic matrix to be detected. Larger biomolecules are known to be thermally labile and they need the controlled energy transfer from an organic matrix to be analyzed by the laser desorption method.

- 1
2
3
4
5
6
7
8
9
10
11
12
13
14
15
16
17
18
19
20
21
22
23
24
- B. Most of the pSi, SiNW and SiNP surfaces are modified, while half of the published work on nano Si does not use surface modification. This suggests that dry fabrication techniques produce stable surfaces, while wet chemistry fabrication techniques produce surfaces that need stabilization.
- C. Si LDI-MS has first appeared as DIOS (pSi), then evolved into NIMS (pSi) and lately it is appearing as nanostructured silicon LDI. The use of matrix is reflected on the evolution of Si LDI-MS as organic matrices were used together with pSi and SiNP but are less and less used together with newer nanostructured Si substrates. We envision that matrix-free strategies will be the LDI strategy of choice in the future.

25 **6. Conclusion**

26
27
28
29
30
31
32
33
34
35
36
37
38
39
40
41
42
43
44
45
46
47
48
49
50
51
52
53
54
55
56
57
58
59
60
61
62
63
64
65

The extensive variety of silicon nanostructures used for MS applications draws attention to the major prerequisites for a successful LDI-MS analysis. For this, we conclude that the basic requirements for any silicon-based substrates are: (1) to absorb UV laser irradiation without deteriorate from it, (2) to provide a surface for easy functionalization, (3) to be stable under vacuum, (4) to improve and enhance the analyte ionizability, (5) to not cause interferences or clusters with the target analyte, (6) to be easy to fabricate, (7) to allow reproducible results and finally, (8) to be cheap. Taking into consideration that silicon technology (regardless of the field of study) is constantly advancing, fabrication and functionalization of silicon-based substrates will rapidly evolve and have a great impact in the mass spectrometry imaging field.

Supporting Information

Supporting Information is available from the Wiley Online Library or from the author.

Acknowledgements

The authors want to acknowledge the financial support of the Spanish Ministry of Economy and Competitiveness (MINECO) through projects TEC2015-69076-P and S. A. Iakab's pre-doctoral grant No. BES-2016-076483, the Spanish Ministry of Science, Innovation and Universities (MICIN) through projects RTI2018-096061-B-I00 and M. Garcia-Altares' post-doctoral grant IJCI-2017-33438, and the 2017-SGR-1119 grant awarded recently by the Agency for Management of University and Research Grants of the Generalitat de Catalunya (AGAUR).

Received: ((will be filled in by the editorial staff))

Revised: ((will be filled in by the editorial staff))

Published online: ((will be filled in by the editorial staff))

References

- 1
2 [1] D. S. Cornett, M. L. Reyzer, P. Chaurand, R. M. Caprioli, *Nat. Methods* **2007**, *4*, 828.
3
4 [2] H. N. Abdelhamid, *TrAC - Trends Anal. Chem.* **2017**, *89*, 68.
5
6 [3] L. A. McDonnell, R. M. A. Heeren, *Mass Spectrom. Rev.* **2007**, *26*, 606.
7
8 [4] J. L. Norris, R. M. Caprioli, *PROTEOMICS - Clin. Appl.* **2013**, *7*, 733.
9
10 [5] C.-K. Chiang, W.-T. Chen, H.-T. Chang, *Chem. Soc. Rev.* **2011**, *40*, 1269.
11
12 [6] C. Gregson, *Biosci. Horizons* **2009**, *2*, 134.
13
14 [7] E. Gemperline, S. Rawson, L. Li, *Anal. Chem.* **2014**, *86*, 10030.
15
16 [8] N. Ogrinc Potočnik, T. Porta, M. Becker, R. M. A. Heeren, S. R. Ellis, *Rapid Commun.*
17
18 *Mass Spectrom.* **2015**, *29*, 2195.
19
20 [9] D. S. Peterson, *Mass Spectrom. Rev.* **2007**, *26*, 19.
21
22 [10] L. Qiao, B. Liu, H. H. Girault, *Nanomedicine* **2010**, *5*, 1641.
23
24 [11] C. Y. Shi, C. H. Deng, *Analyst* **2016**, *141*, 2816.
25
26 [12] K. P. Law, J. R. Larkin, *Anal. Bioanal. Chem.* **2011**, *399*, 2597.
27
28 [13] Y. E. Silina, D. A. Volmer, *Analyst* **2013**, *138*, 7053.
29
30 [14] J. Sekuła, J. Nizioł, W. Rode, T. Ruman, *Anal. Chim. Acta* **2015**, *875*, 61.
31
32 [15] M. Dufresne, A. Thomas, J. Breault-Turcot, J.-F. Masson, P. Chaurand, *Anal. Chem.*
33
34 **2013**, *85*, 3318.
35
36 [16] H. Kawasaki, T. Ozawa, H. Hisatomi, R. Arakawa, *Rapid Commun. Mass Spectrom.*
37
38 **2012**, *26*, 1849.
39
40 [17] Y. Gholipour, S. L. Giudicessi, H. Nonami, R. Erra-Balsells, *Anal. Chem.* **2010**, *82*,
41
42 5518.
43
44 [18] A. Y. Lim, J. Ma, Y. C. F. Boey, *Adv. Mater.* **2012**, *24*, 4211.
45
46 [19] Y. He, C. Fan, S. T. Lee, *Nano Today* **2010**, *5*, 282.
47
48 [20] F. Peng, Y. Su, Y. Zhong, C. Fan, S. T. Lee, Y. He, *Acc. Chem. Res.* **2014**, *47*, 612.
49
50 [21] J. J. Thomas, Z. Shen, J. E. Crowell, M. G. Finn, G. Siuzdak, *Proc. Natl. Acad. Sci. U.*
51
52
53
54
55
56
57
58
59
60
61
62
63
64
65

- S. A. **2001**, 98, 4932.
- [22] T. R. Northen, O. Yanes, M. T. Northen, D. Marrinucci, W. Uritboonthai, J. Apon, S. L. Golledge, A. Nordström, G. Siuzdak, *Nature* **2007**, 449, 1033.
- [23] J. Wei, J. M. Buriak, G. Siuzdak, *Nature* **1999**, 399, 243.
- [24] N. Budimir, J. C. Blais, F. Fournier, J. C. Tabet, *Rapid Commun. Mass Spectrom.* **2006**, 20, 680.
- [25] A. G. Cullis, L. T. Canham, P. D. J. Calcott, *J. Appl. Phys.* **1997**, 82, 909.
- [26] T. Guinan, C. Della Vedova, H. Kobus, N. H. Voelcker, *Chem. Commun.* **2015**, 51, 6088.
- [27] L. Chen, Z.-T. Chen, J. Wang, S.-J. Xiao, Z.-H. Lu, Z.-Z. Gu, L. Kang, J. Chen, P.-H. Wu, Y.-C. Tang, J.-N. Liu, *Lab Chip* **2009**, 9, 756.
- [28] H. Yan, A. Ahmad-Tajudin, M. Bengtsson, S. Xiao, T. Laurell, S. Ekström, *Anal. Chem.* **2011**, 83, 4942.
- [29] J. Li, C. Lu, X. K. Hu, X. Yang, A. V. Loboda, R. H. Lipson, *Int. J. Mass Spectrom.* **2009**, 285, 137.
- [30] X. Yongsheng, T. R. Scott, K. T. Darrell, T. Jia-Yuan, H. Lin, *J. Phys. Chem. C* **2009**, 113, 3076.
- [31] M. Gaspari, M. M. Cheng, R. Terracciano, X. Liu, A. J. Nijdam, L. Vaccari, E. Fabrizio, E. F. Petricoin, L. A. Liotta, G. Cuda, S. Venuta, M. Ferrari, *J. Proteome Res.* **2006**, 5, 1261.
- [32] Y. Goto, N. Mizoshita, Y. Yamada, Y. Maegawa, J. Amano, S. Inagaki, *Microporous Mesoporous Mater.* **2018**, 268, 125.
- [33] T. Guinan, M. Ronci, H. Kobus, N. H. Voelcker, *Talanta* **2012**, 99, 791.
- [34] Y.-Q. Chen, F. Bi, S.-Q. Wang, S.-J. Xiao, J.-N. Liu, *J. Chromatogr. B* **2008**, 875, 502.
- [35] S. a Trauger, E. P. Go, Z. Shen, J. V Apon, B. J. Compton, E. S. P. Bouvier, M. G. Finn, G. Siuzdak, *Anal. Chem.* **2004**, 76, 4484.

- 1
2
3
4
5
6
7
8
9
10
11
12
13
14
15
16
17
18
19
20
21
22
23
24
25
26
27
28
29
30
31
32
33
34
35
36
37
38
39
40
41
42
43
44
45
46
47
48
49
50
51
52
53
54
55
56
57
58
59
60
61
62
63
64
65
- [36] M. Ronci, D. Rudd, T. Guinan, K. Benkendorff, N. H. Voelcker, *Anal. Chem.* **2012**, *84*, 8996.
- [37] D. Rudd, M. Ronci, M. R. Johnston, T. Guinan, N. H. Voelcker, K. Benkendorff, *Sci. Rep.* **2015**, *5*, 1.
- [38] T. M. Guinan, D. Neldner, P. Stockham, H. Kobus, C. B. Della Vedova, N. H. Voelcker, *Drug Test. Anal.* **2017**, *9*, 769.
- [39] T. Guinan, M. Ronci, R. Vasani, H. Kobus, N. H. Voelcker, *Talanta* **2015**, *132*, 494.
- [40] H. Zhou, S. Xu, M. Ye, S. Feng, C. Pan, X. Jiang, X. Li, G. Han, Y. Fu, H. Zou, *J. Proteome Res.* **2006**, *5*, 2431.
- [41] H. Yan, N. Xu, W.-Y. Huang, H.-M. Han, S.-J. Xiao, *Int. J. Mass Spectrom.* **2009**, *281*, 1.
- [42] O. J. R. Gustafsson, T. M. Guinan, D. Rudd, H. Kobus, K. Benkendorff, N. H. Voelcker, *Rapid Commun. Mass Spectrom.* **2017**, *31*, 991.
- [43] G. J. Patti, L. P. Shriver, C. A. Wassif, H. K. Woo, W. Uritboonthai, J. Apon, M. Manchester, F. D. Porter, G. Siuzdak, *Neuroscience* **2010**, *170*, 858.
- [44] S. Tuomikoski, K. Huikko, K. Grigoras, P. Ostman, R. Kostianen, M. Baumann, J. Abian, T. Kotiaho, S. Franssila, *Lab Chip* **2002**, *2*, 247.
- [45] M. J. Sweetman, M. Ronci, S. R. Ghaemi, J. E. Craig, N. H. Voelcker, *Adv. Funct. Mater.* **2012**, *22*, 1158.
- [46] X. Li, J. Tan, J. Yu, J. Feng, A. Pan, S. Zheng, J. Wu, *Anal. Chim. Acta* **2014**, *849*, 27.
- [47] J. Wang, M. Jie, H. Li, L. Lin, Z. He, S. Wang, J. M. Lin, *Talanta* **2017**, *168*, 222.
- [48] T. N. Moening, V. L. Brown, L. He, *Anal. Methods* **2016**, *8*, 8234.
- [49] G. J. Patti, H. K. Woo, O. Yanes, L. Shriver, D. Thomas, W. Uritboonthai, J. V Apon, R. Steenwyk, M. Manchester, G. Siuzdak, *Anal. Chem.* **2009**, *82*, 4271.
- [50] J. Gao, M. De Raad, B. P. Bowen, R. N. Zuckermann, T. R. Northen, *Anal. Chem.* **2016**, *88*, 1625.

- 1
2
3
4
5
6
7
8
9
10
11
12
13
14
15
16
17
18
19
20
21
22
23
24
25
26
27
28
29
30
31
32
33
34
35
36
37
38
39
40
41
42
43
44
45
46
47
48
49
50
51
52
53
54
55
56
57
58
59
60
61
62
63
64
65
- [51] J. Gao, K. B. Louie, P. Steinke, B. P. Bowen, M. De Raad, R. N. Zuckermann, G. Siuzdak, T. R. Northen, *Anal. Chem.* **2017**, *89*, 6521.
- [52] J. Heinemann, K. Deng, S. C. C. Shih, J. Gao, P. D. Adams, A. K. Singh, T. R. Northen, *Lab Chip* **2017**, *17*, 323.
- [53] Y. Chen, H. Chen, A. Aleksandrov, T. M. Orlando, *J. Phys. Chem. C* **2008**, *112*, 6953.
- [54] H. K. Woo, T. R. Northen, O. Yanes, G. Siuzdak, *Nat. Protoc.* **2008**, *3*, 1341.
- [55] M. Dupré, S. Cantel, J. O. Durand, J. Martinez, C. Enjalbal, *Anal. Chim. Acta* **2012**, *741*, 47.
- [56] H. Chen, C. Deng, X. Zhang, *Angew. Chemie Int. Ed.* **2010**, *49*, 607.
- [57] S. Liu, H. Chen, X. Lu, C. Deng, X. Zhang, P. Yang, *Angew. Chemie - Int. Ed.* **2010**, *49*, 7557.
- [58] H. Chen, S. Liu, H. Yang, Y. Mao, C. Deng, X. Zhang, P. Yang, *Proteomics* **2010**, *10*, 930.
- [59] Y. Xiong, C. Deng, X. Zhang, P. Yang, *ACS Appl. Mater. Interfaces* **2015**, *7*, 8451.
- [60] X. Zhu, L. Wu, D. C. Mungra, S. Xia, J. Zhu, *Analyst* **2012**, *137*, 2454.
- [61] X. Wen, S. Dagan, V. H. Wysocki, *Anal. Chem.* **2007**, *79*, 434.
- [62] S. Dagan, Y. Hua, D. J. Boday, A. Somogyi, R. J. Wysocki, V. H. Wysocki, *Int. J. Mass Spectrom.* **2009**, *283*, 200.
- [63] M. Hong, X. Zhou, J. Li, Y. Tian, J. Zhu, *Anal. Chem.* **2009**, *81*, 8839.
- [64] E. P. Go, J. V. Apon, G. Luo, A. Saghatelian, R. H. Daniels, V. Sahi, R. Dubrow, B. F. Cravatt, A. Vertes, G. Siuzdak, *Anal. Chem.* **2005**, *77*, 1641.
- [65] G. Luo, Y. Chen, H. Daniels, R. Dubrow, A. Vertes, *J. Phys. Chem. B* **2006**, *110*, 13381.
- [66] A. Muck, T. Stelzner, U. Hübner, S. Christiansen, A. Svatos, *Lab Chip* **2010**, *10*, 320.
- [67] G. Piret, H. Drobecq, Y. Coffinier, O. Melnyk, R. Boukherroub, *Langmuir* **2010**, *26*, 1354.

- 1
2
3
4
5
6
7
8
9
10
11
12
13
14
15
16
17
18
19
20
21
22
23
24
25
26
27
28
29
30
31
32
33
34
35
36
37
38
39
40
41
42
43
44
45
46
47
48
49
50
51
52
53
54
55
56
57
58
59
60
61
62
63
64
65
- [68] F. Lapierre, G. Piret, H. Drobecq, O. Melnyk, Y. Coffinier, V. Thomy, R. Boukherroub, *Lab Chip* **2011**, *11*, 1620.
- [69] M. Dupré, Y. Coffinier, R. Boukherroub, S. Cantel, J. Martinez, C. Enjalbal, *J. Proteomics* **2012**, *75*, 1973.
- [70] R. A. Picca, C. D. Calvano, M. J. Lo Faro, B. Fazio, S. Trusso, P. M. Ossi, F. Neri, C. D'Andrea, A. Irrera, N. Cioffi, *J. Mass Spectrom.* **2016**, 849.
- [71] W. Y. Chen, J. T. Huang, Y. C. Cheng, C. Chien, C. W. Tsao, *Anal. Chim. Acta* **2011**, *687*, 97.
- [72] H. Z. Alhmoud, T. M. Guinan, R. Elnathan, H. Kobus, N. H. Voelcker, *Analyst* **2014**, *139*, 5999.
- [73] C. W. Tsao, Z. J. Yang, *ACS Appl. Mater. Interfaces* **2015**, *7*, 22630.
- [74] P. Y. Chen, C. Y. Hsieh, C. J. Shih, Y. J. Lin, C. W. Tsao, Y. L. Yang, *J. Nat. Prod.* **2018**, *81*, 1527.
- [75] B. Gulbakan, D. Park, M. Kang, K. Kececi, C. R. Martin, D. H. Powell, W. Tan, *Anal. Chem.* **2010**, *82*, 7566.
- [76] Y. Wang, Z. Zeng, J. Li, L. Chi, X. Guo, N. Lu, *J. Am. Soc. Mass Spectrom.* **2013**, *24*, 66.
- [77] N. J. Morris, H. Anderson, B. Thibeault, A. Vertes, M. J. Powell, T. T. Razunguzwa, *RSC Adv.* **2015**, *5*, 72051.
- [78] A. R. Korte, N. J. Morris, A. Vertes, *Anal. Chem.* **2019**, *91*, 3951.
- [79] Y. Chen, A. Vertes, *Anal. Chem.* **2006**, *78*, 5835.
- [80] R. Daniels, S. Dikler, E. Li, C. Stacey, *J. Assoc. Lab. Autom.* **2008**, *13*, 314.
- [81] K. Chughtai, R. M. A. Heeren, *Chem. Rev.* **2011**, *110*, 3237.
- [82] M. Karas, D. Bachmann, F. Hillenkamp, *Anal. Chem.* **1985**, *57*, 2935.
- [83] K. Dreisewerd, *The desorption process in MALDI*; 2003; Vol. 103.
- [84] R. Zenobi, R. Knochenmuss, *Mass Spectrom. Rev.* **1998**, *17*, 337.

- 1
2
3
4
5
6
7
8
9
10
11
12
13
14
15
16
17
18
19
20
21
22
23
24
25
26
27
28
29
30
31
32
33
34
35
36
37
38
39
40
41
42
43
44
45
46
47
48
49
50
51
52
53
54
55
56
57
58
59
60
61
62
63
64
65
- [85] M. Karas, R. Krüger, *Chem. Rev.* **2003**, *103*, 427.
- [86] W. C. Chang, L. C. L. Huang, Y. S. Wang, W. P. Peng, H. C. Chang, N. Y. Hsu, W. Bin Yang, C. H. Chen, *Anal. Chim. Acta* **2007**, *582*, 1.
- [87] T. W. Jaskolla, M. Karas, *J. Am. Soc. Mass Spectrom.* **2011**, *22*, 976.
- [88] J. A. Stolee, B. N. Walker, V. Zorba, R. E. Russo, A. Vertes, *Phys. Chem. Chem. Phys.* **2012**, *14*, 8453.
- [89] M. Muthu, S. Chun, H.-F. Wu, M. W. Duncan, J. Gopal, *J. Mass Spectrom.* **2018**, 525.
- [90] R. A. Picca, C. D. Calvano, N. Cioffi, F. Palmisano, *Nanomaterials* **2017**, *7*, 75.
- [91] J. L. Norris, R. M. Caprioli, *Chem Rev.* **2013**, *113*, 2309.
- [92] Y. J. Lee, D. C. Perdian, Z. Song, E. S. Yeung, B. J. Nikolau, *Plant J.* **2012**, *70*, 81.
- [93] J. Kriegsmann, M. Kriegsmann, R. Casadonte, *Int. J. Oncol.* **2015**, *46*, 893.

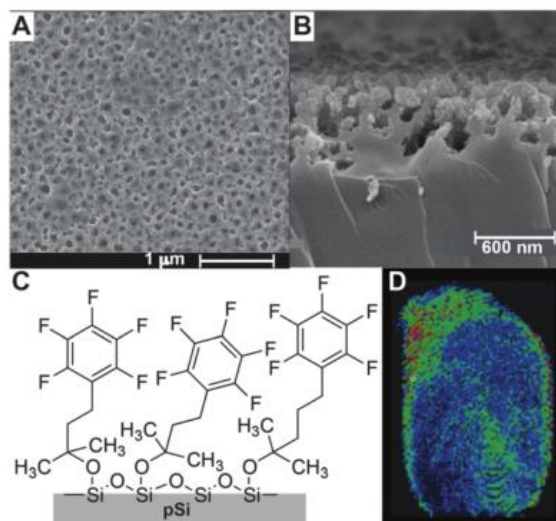


Figure 1. SEM of a DIOS chip in (A) the top view and (B) the cross-sectional view. (C) The schematic of pSi functionalized with F5PhPr and (D) DIOS- MSI of fingerprint sweat at 200 μm resolution. Reprinted with permission ^[26], Copyright 2015 © The Royal Society of Chemistry

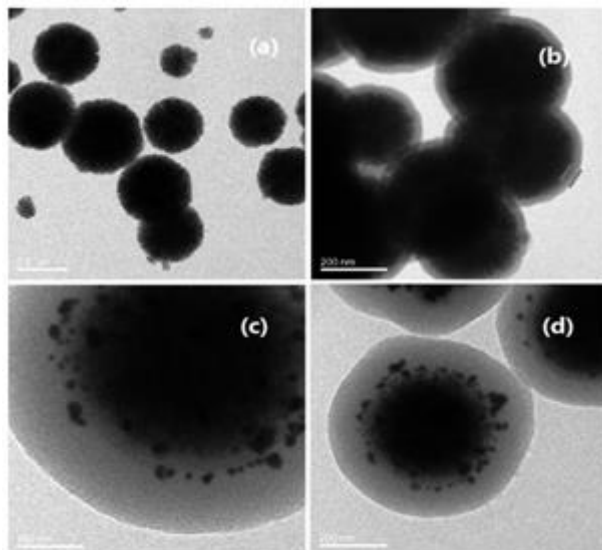


Figure 2. Electron microscope images of silicon nanoparticles. Reprinted and adapted with permission^[59]. Copyright © 2015 American Chemical Society

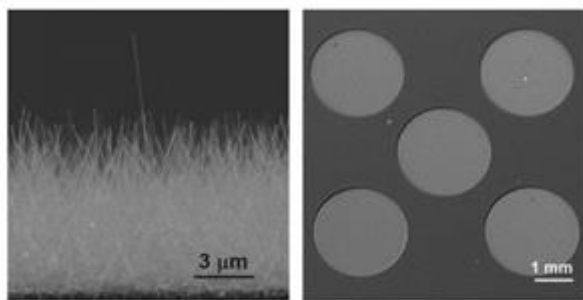


Figure 3. Electron microscope images of silicon nanowires. Reprinted and adapted with permission^[66], Copyright © The Royal Society of Chemistry 2010

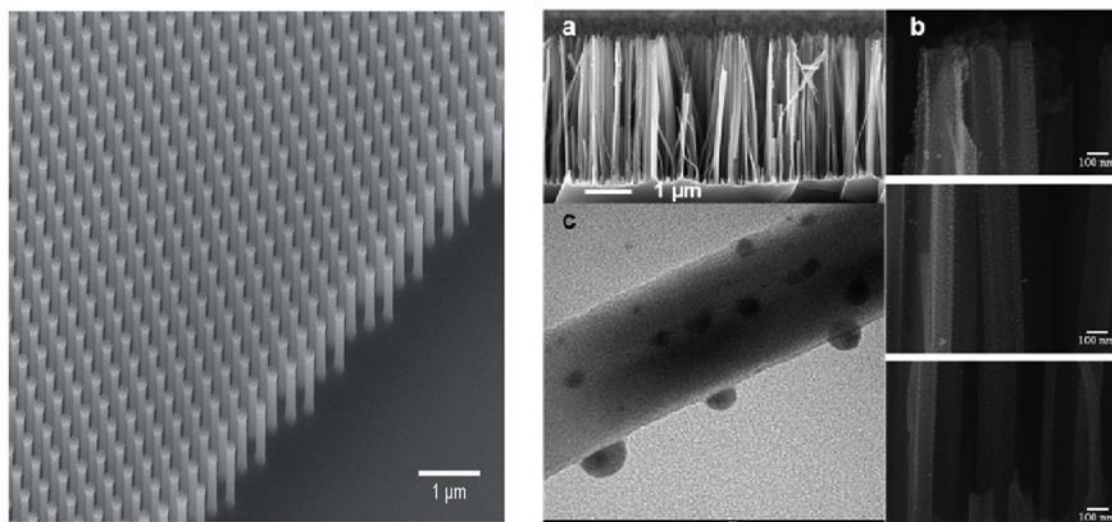


Figure 4. Electron microscope images of silicon nanopost array^[77] (left) and Ag-functionalized silicon nanowire array^[70] (right). Reprinted and adapted with permission, Copyright © 2015 The Royal Society of Chemistry and Copyright © 2016 John Wiley & Sons, Ltd

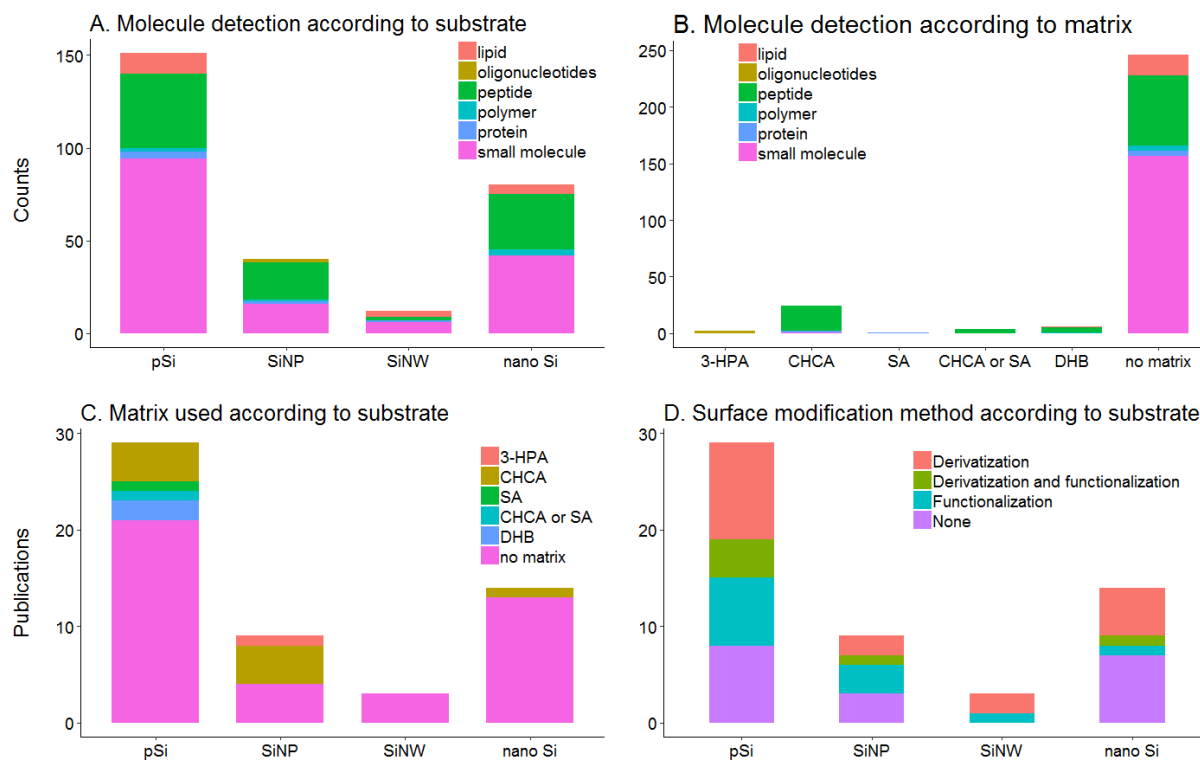


Figure 5. Bar charts summarizing the detection strategies used in the reviewed publications presented in this work.

Table 1. Functionalization methods of porous silicon substrates for detection of biomolecules

Surface modification methods ^{a)}	Detected Molecules and Limit of Detection (LOD if available)	Matrix ^{b)}	Ref
N/A	choline (40 μ M), BSA, FHV, adenovirus penton protein, β -lactoglobulin	-	[21]
N/A	four-residue peptide (MRFA), des-arg-bradykinin, bradykinin, angiotensin, adrenocorticotrophic hormone (2 pmol each); caffeine, antiviral drug WIN, reserpine (1 pmol each); N-octyl β -D-glucopyranoside	-	[23]
N/A	prednisolone, dalargin, bradykinin, adrenocorticotrophic hormone (ACTH) 1–17	-	[29]
N/A	4-amino-1-benzylpyridinium bromide (0.5 mM), 1,2-dihexadecanoyl-sn-glycero-3-phosphocholine (0.01 mM), angiotensin III (2.5 mg/mL)	-	[30]
N/A	heptadecanoic acid, stearic acid, nonadecanoic acid, arachidic acid, heneicosanoic acid, behenic acid (2 nmol each)	-	[24]
Silylation with chlorosilane and addition of physically adsorbed initiator	verapamil (700 ymol), BSA (500 amol), phospholipids; bradykinin 2-9, bradykinin 1-7 and neurotensin (1 fmol peptide array), phosphatidylcholine, phosphatidylethanolamine, codeine (15 ng/ml)	-	[22]
Silylation using various silylating agents (TMS, C8, NH ₂)	<u>perfluorophenyl silylated pSi</u> : midazolam (200 fmol); propafenone (200 fmol); verapamil (200 fmol), des-Arg9-bradykinin (800 ymol) <u>amine silylated pSi</u> : sucrose (25 pmol); maltotriose (25 pmol) phenylalanine, alanine, isoleucine/leucine, glutamic acid	-	[35]
Silylation with F5PhPr	tyrindoxyl sulfate; 6,6'-dibromoindigo	-	[36]
	murexine; tyrindoxyl hydrogen sulfate; tyrindoleninone; Tyrian purple	-	[37]
	cholesterol; nicotine; methamphetamine; amphetamine; nonanoic acid; methadone; EDDP; codeine	-	[26]
Silylation with F5PhPr, F13 and F17	MA (2.88 ng/mL); MDMA (0.66 ng/mL); cocaine (0.86 ng/mL)	-	[33]
Silylation with neat BisF17	methadone (14.74ng/mL in saliva; 18.84ng/mL in plasma; 19.50ng/mL in urine)	-	[38]
Silylation with neat F17and BisF17	methadone (100 ng/mL); oxycodone (2.5 ng/mL in water and 10 ng/mL in PBS); flunitrazepam (100 ng/mL); MDMA (100 ng/mL); cocaine (100 ng/mL)	-	[39]
Two levels of derivatization (aminopropyl then phosphonate) and functionalization with Zr	phosphopeptides from α -casein, β -casein and BSA	DHB	[40]
Two levels of functionalization (Ag and 4-ATP)	TPyP (5.2 fmol); oxytocin (0.4 pmol); PEG 400 (3 pmol); PEG 2300 (30 pmol)	-	[41]
Functionalization with nanometer Ag layer	fingermark: DTDMA C16/C16; DTDMA C16/C18; DTDMA C18/C18; TAG 48:1; oleic acid; stearic acid; WE 36:1; Behentrimonium tissue section: PC head group; oleic acid; stearic acid; 6,6'-dibromoindirubin (Tyrian purple); cholesterol	-	[42]
Functionalization with AgNO ₃ solution and addition of physically adsorbed initiator	cholesterol and 7DHC	-	[43]
Two levels of derivatization (10 undecenoic acid and ethyl undecenoate)	buprenorphine (100 fmol); midazolam (150 fmol); psilocin (5 pmol); propranolol (4 pmol); 1-Naphthalene methylamine (6 pmol); 2-Naphthylacetic acid (5 pmol); dichloromethyl phosphonate (60 pmol); dichloromethylene bisphosphonate (40	-	[44]

	pmol); Leu-Enkephalin-Arg (4 pmol); Des-Arg1-Bradykinin (4 pmol); Substance P (3 pmol)		
Derivatization by RIE etching in gas mixture O ₂ /CF ₄ and toluene wash	peptide and oligosaccharide molecules	-	[32]
Two levels of derivatization (undecylenic acid and NHS) and functionalization with BNP antibodies	different BNP concentration solutions prepared in PBS buffer and in human plasma (10pg/mL)	CHCA	[34]
Two levels of silylation (alkene 1 and alkene 3) and functionalization with FITC-BSA or FN	tryptic peptides of fibronectin from human neuroblastoma cell line SK-N-SH	CHCA	[45]
Four levels of derivatization (OH, carboxyl, NHS and NTA) and functionalization with Ni ²⁺	Trx-urodilatin(1 pM)	SA	[27]
Functionalization with angiotensin I antibodies	angiotensin I (1 nM in diluted plasma)	CHCA	[28]
Derivatization with pentane	Substance P, renin substrate tetrapeptide, angiotensin I (ng/ml standard solutions) and calcitonin	CHCA SA	[31]
Functionalization with electrochemically deposited Au	model sample consisting of HRP digest (100 mg/mL); excess BSA; serum peptides, insulin	CHCA	[46]
Functionalization with AuNPs	GSH (10 µg/mL in standard solution), GSH (healty and Irinotecan-treated Caco-2 cells) and l-cysteine (10 µg/mL)	-	[47]
Addition of BisF17 initiator coating	angiotensin III, bradykinin, and angiotensin I (0.3 µM each), lipid species	DHB	[48]
Functionalization with AgNO ₃ solution and addition of initiator coating	testosterone, vitamin D3, glucose (300 fmol), sucrose (500 fmol), maltotriose (800 amol), maltohexaose, maltoheptaose, β- and γ-cyclodextrin; trans-androsterone, progesterone, corticosterone, and prednisone (500 fmol each), cholesterol	-	[49]
Addition of BisF17 initiator coating on black silicon*	spermidine, arginine, adenosine, palmitoylcarnitine, verapamil, STAL-2 (100 fmol-10 pmol), Bradykinin	-	[50]
Addition of BisF17 initiator coating	arginine, palmitoylcarnitine, streptomycin, bradykinin, angiotensin, ACTH residues ("clip" 1-17, 18-39, 7-38), insulin B, neurotensin	-	[51]
N/A ^{c)}	dextromethorphan and CeIE-CBM3a enzymatic assay	-	[52]
N/A	arginine, tryptophan, histidine, methionine, glutamine, and glycine (5 µg/mL each)	-	[53]

^{a)} N/A = information not available; ^{b)} - matrix-free method; ^{c)} not porous silicon

Table 2. Silicon nanostructures: fabrication, functionalization and applications

	Fabrication Methods	Surface modification methods ^{a)}	Analyzed Molecules	Matrix ^{b)}	Ref.
Nanoparticles and nano-powders	Sol-gel synthesis (SiO ₂ NPs)	N/A	48 sequences from synthetic peptides mimicking protein digests	-	[55]
	Sol-gel synthesis (magnetite core-shell Fe ₃ O ₄ @SiO ₂ microspheres)	Modification with MPS and polymerization of MMA	standard peptide angiotensin II (DRVYIHPF), standard protein cytochrome C	CHCA	[56]
		Functionalization with Cu ²⁺ ions by surface grafting	angiotensin II, tryptic BSA digest, peptides from human serum and urine	CHCA	[57]
		CSNPs dried and calcined in N ₂	angiotensin II, MYO digest and BSA digest	CHCA	[58]
		Functionalization with Au	human insulin, immunoglobulin G, human serum albumin, α 1- antitrypsin, horseradish peroxidase, β -casein, lysozyme, cytochrome C	CHCA	[59]
	AuNPs coated with an ultrathin silica shell	Stabilization of Au@SiO ₂ CSNPs by growth of the silica shell	aspartic acid, N-(4-hydroxyphenyl)acetamide, 2-(2-methyl-5-nitro-1H-imidazole-1-yl)ethanol, norfloxacin, amoxicillin, erythromycin, PEG1000, roxithromycin and temporin-SHf	-	[60]
	Particles purchased from distributors	Etching with HF, oxidation with HNO ₃ and derivatization with PFP, PHP, or TMS	peptides leucine enkephalin (200 μ g/mL), angiotensin II (DRVYIHPF) (100 μ g/mL), nucleobase adenine (400 μ g/mL), propafenone (10 pmol/ μ L), verapamil (10 pmol/ μ L), trioctylamine (80 μ g/mL) morphine and propafenone from spiked urine ametryn and altretamine from spiked soil	-	[61]
			Oxidation with HNO ₃ and silylation with C10, C6 or C3	2-methyl, 4-methyl, 3-methoxy, 4-methoxy and 4-chloro benzylpyridiniums	-
		Functionalization with Au by dipping in AuNP solution	surface-confined DNA: ss-DNA and ds-DNA	3-HPA	[63]
	Nanowires	Au nanocluster-catalyzed vapor-liquid-solid (VLS) growth mechanism	Oxidation with ozone and silylation with PFP	cocaine (3 μ M spiked saliva), BSA and FHV tryptic digests (1 μ M), and des-Arg9-bradykinin, midazolam, propafenone, and verapamil (all 1 mg/mL aqueous solution)	-
			chloride salts of seven benzyl-substituted benzylpyridinium ions (70 μ M standard solution)	-	[65]
Doping with LiOH after sample deposition			diglycerides, tristearin, tripalmitin, fatty acids and glyceride		[66]
Nanostructured surfaces	Chemical etching (variations on HF/AgNO ₃ aq. solution)	Oxidation by UV/ozone and silylation with OTS, FDTS, or ODCS	peptide mixture: Des-Arg-bradykinin, angiotensin I, fibrinopeptide B and neurotensin (10 fmol/ μ L), verapamil (5 fmol/ μ L) and Sutent (10 fmol/ μ L)	-	[67]
		Silylation with OTS	peptide mixture (fmol/mL): Des-Arg-Bradykinin, angiotensin I, fibrinopeptide B and neurotensin 15 tryptic peptides and 14 Lys-N peptides	-	[68] [69]
		Functionalization with AgNPs by pulsed laser deposition	linoleic acid, oleic acid, arachidonic acid, squalene, diacylglycerol	-	[70]
	Metal-assisted chemical etching (using Ag or Au nanostructures and aqueous HF etching solution)	N/A	single model peptide sample des-Arg9 Bradykinin (1 pM)	-	[71]
		Oxidation by ozone and silylation with F13	methadone (100 ng/mL aqueous solution), EDDP from clinical samples of blood plasma, saliva, and urine and peptide mixture: angiotensin I, angiotensin II, substance P, bombesin, ACTH clip 1–17, ACTH clip 18–39, somatostatin 28	-	[72]
		Oxidation by O ₂ plasma and AuNP grafting by immersion in HF/HAuCl ₄ solution	glucose (100 μ M aqueous solution) (50 mM spiked urine samples)	-	[73]

		Au deposited by e-beam evaporation, immersion in 1:1:1 volume ratio of HF/H ₂ O ₂ /EtOH solution	natural products in microbial interactions: metabolites, peptides	-	[74]
	Reactive ion etching (mask and gas mixture plasma)	N/A	adenosine, Pro-Leu-Gly tripeptide, and bradykinin, fentanyl, BSA digest and standard carnitine metabolite cocktail	-	[75]
		N/A	PEG, bradykinin, Arg, and TMZ (100 μM in standard solutions) and glucose from urine samples from healthy and diabetic patients	CHCA DHB	[76]
		N/A	buprenorphine, norbuprenorphine, ropivacaine, amiodarone, chlorpheniramine, fentanyl, clonidine, nordiazepam, metoprolol, verapamil	-	[77]
		photopatterning, RIE etching and cleaning using standard microelectronics steps	metabolites from hepatocyte extracts or urine aliquots	-	[78]
	Laser irradiation (in air, SF ₆ gas, or DI water)	N/A	angiotensin I, bovine insulin, PPG1000 and PEG400 (0.5 nmol/μL)	-	[79]
	Commercial NALDI targets	hydrophobic organic coating	clonidine, propranolol, quinidine, papaverine, verapamil, ketoconazol, prazosin, haloperidol	-	[80]

^{a)} N/A= information not available; ^{b)} - no matrix used



Xavier Correig received his PhD in Telecommunication Engineering from the Polytechnic University of Catalonia. He currently serves as Professor at the Universitat Rovira i Virgili. Since 2007 he directs the Metabolomics Platform, a scientific infrastructure owned by the URV and the Spanish research institute on diabetes and metabolic diseases (CIBERDEM), whose mission is to provide metabolomic analysis to clinical and biomedicine research groups. Present interests are development of new solid-state surfaces and signal processing algorithms for LDI-MS Imaging.



Stefania Alexandra Iakab received her bachelors' degree in Medical Physics and masters' degree in Biomaterials from the Babes-Bolyai University, Cluj-Napoca, Romania. She is currently a PhD student under the guidance of Prof. Xavier Correig within the Department of Electronic Engineering at the Rovira i Virgili University. Her current research focus is developing novel nanostructured surfaces for molecular imaging applications relevant to the clinical, pharmaceutical and environmental areas.



Pere Ràfols is a post-doc researcher in the Department of Electronic Engineering at the Rovira i Virgili University. He received his PhD for his work focused on the development of novel techniques for mass spectrometry imaging (MSI). He contributed to technologies to apply MSI at metabolomics studies. This includes the research of sputtering-based metal-coating for MSI analysis of low-weight compounds and the development of open-source software tools for MSI data processing and visualization. He is currently focused on the development of efficient software tools for MSI data analysis and experimental validation.

Supporting Information

Silicon-based Laser Desorption Ionization Mass Spectrometry for the Analysis of Biomolecules: A Progress Report*Stefania Alexandra Iakab, Pere Rafols, María García-Altare, Oscar Yanes, Xavier Correig****Table S1.** Electrochemical etching fabrication methods

Pre-etch cleaning process	Current density (mA/cm ²)	Etching solution (vol/vol)	Time (sec)	Illumination	Teflon cell	Ref.
n-type	71	1:1 EtOH/49% HF	60-180	300-W tungsten filament bulb	N/A	[23]
p-type	37	1:1 EtOH/49% HF	10800	in the dark	N/A	[23]
5% HF/ethanol solution and then rinsed in deionized water, acetone, and methanol	40	1:1 EtOH/48% HF	300 prior laser and 900 with laser	4 ns pulses of a 355 nm frequency-tripled Nd:YAG laser operating at a 20Hz repetition rate and with an intensity of 4 W/cm ²	Yes	[29]
N/A	5	25% EtOH/HF	60	white-light 50 mW/cm ²	N/A	[21]
Methanol wash 3-5 times	48	EtOH /25%HF	1800	N/A	Yes	[22]
N/A	10 - 50	1:1 EtOH/50%HF	N/A	300–500 W halogen lamp	Yes	[44]
N/A	5	25% EtOH/HF	120	white light	N/A	[35]
N/A	4	2:3 EtOH/49%HF	100	250 W tungsten filament bulb	Yes	[40]
Boiled in 3:1 (v/v) concentrated H ₂ SO ₄ /30% H ₂ O ₂ for 30min and then rinsed extensively with Milli-Q water.	100	1:3 EtOH/40%HF	180	N/A	N/A	[34]
Cleaned with 3:1 (v/v) H ₂ SO ₄ /H ₂ O ₂ for 30 min, rinsed with copious amounts of water and absolute ethanol, and then immersed in water prior to the etching procedure	60	1:3 EtOH/40%HF	600	In the dark	Yes	[41]
piranha solution for 30 min rinsed with nano- pure water, and blown dry with nitrogen gas	300	EtOH /25%HF	1800	N/A	N/A	[43]
N/A	20	1:1 EtOH/HF	120	fiber optic light source*	Yes	[36]
Rinsed with methanol, acetone and DCM	20	1:3 EtOH/48%HF	300	N/A	Yes	[45]

Sonicated in 99.9% methanol and dried under a stream of nitrogen.	4	1:1 EtOH/HF	120	fiber optic light source*	Yes	[33]
N/A	20	1:1 EtOH/HF	120	fiber optic light source*	Yes	[26]
N/A	27	1:2 EtOH/HF	300	fiber optic light source*	Yes	[38]
N/A	20	1:1 EtOH/HF	120	fiber optic light source*	Yes	[42]
Sonicated in 99.9% methanol and dried under a stream of nitrogen.	3.2	1:1 EtOH/HF	120	fiber optic light source*	Yes	[39]
N/A	20	1:1 EtOH/HF	120	fiber optic light source*	Yes	[37]
N/A	30	1:4 EtOH/40%HF	30–600	N/A	Yes	[46]
piranha solution for 30 min, thoroughly washed in DI H ₂ O and dried with N ₂	32	EtOH /25%HF	1800	In the dark	N/A	[48]
three solvent baths: trichloroethylene, acetone, and methanol for 15 min sequentially	2360	EtOH /24%HF	120-4800	N/A	Yes	[51]
N/A	N/A	HF/HNO ₃ / H ₂ O (1:3:5) solution	60-240	N/A	N/A	[53]
piranha solution for 30 min and rinsed by nanopure water and dried with N ₂	300	EtOH /25%HF	1800	N/A	Yes	[49]

N/A - information not available; * - no mention of light source or type

Table S2. Stabilization methods of porous silicon substrates

Stabilization method	Ref
ozone oxidation and immersion in diluted aqueous HF solution	[21]
ozone oxidation (hydroxyl-terminated surface)	[35][36][37][33][26][38][39] [42][22]
ozone oxidation and re-etching in ethanol containing 5% HF	[40]
wash with absolute ethanol and drying with nitrogen	[41]
pSi rinsed with a mixture of ethanol–deionized water, then kept in ethanol for 5 min, and finally dried carefully under nitrogen flow.	[44]
pSi was rinsed with pure ethanol and pentane, and then dried with nitrogen	[34]
pSi washed with methanol, acetone and DCM and dried with nitrogen	[45]
Immersion in deionized water, then in ethanol and pentane, dried with nitrogen and stored in a vacuum chamber	[31]

Table S3. Molecules and their respective detection strategies

Molecule	Class	Substrate	Surface modification	Matrix	Ref.	Year
1,2-dihexadecanoyl-sn-glycero-3-phosphocholine (DPPC)	small molecule	pSi	None	no matrix	30	2009
1,4-b-D-cellobiose-probe	peptide	nano Si	None	no matrix	51	2017
14 Lys-N peptides	peptide	nano Si	Derivatization	no matrix	73	2012
15 tryptic peptides	peptide	nano Si	Derivatization	no matrix	73	2012
1-Naphthalene methylamine	small molecule	pSi	Derivatization	no matrix	43	2002
2-(2-methyl-5-nitro-1H-imidazole-1-yl)ethanol	small molecule	SiNP	None	no matrix	59	2012
2-Naphthylacetic acid	small molecule	pSi	Derivatization	no matrix	43	2002
4-amino-1-benzylpyridinium bromide	small molecule	pSi	None	no matrix	30	2009
4-chloro benzylpyridinium salts	small molecule	SiNP	Derivatization	no matrix	61	2009
6,6'-dibromoindigo	small molecule	pSi	Derivatization	no matrix	35	2012
7DHC	small molecule	pSi	Functionalization	no matrix	42	2010
ACTH clip 1–17	peptide	nano Si	Derivatization	no matrix	75	2014
ACTH clip 18–39	peptide	nano Si	Derivatization	no matrix	75	2014
ACTH residues (“clip” 1–17, 18–39, 7–38)	peptide	pSi	None	no matrix	50	2017
adenosine	small molecule	nano Si	None	no matrix	49	2016
adenosine	small molecule	nano Si	None	no matrix	77	2010
adenovirus penton protein	protein	pSi	None	no matrix	21	2001
adrenocorticotrophic hormone	peptide	pSi	None	no matrix	23	1999
Adrenocorticotrophic Hormone (ACTH) 1–17	peptide	pSi	None	no matrix	29	2009
alanine	small molecule	pSi	Derivatization	no matrix	34	2004
altretamine	small molecule	SiNP	Derivatization	no matrix	60	2007
ametryn	small molecule	SiNP	Derivatization	no matrix	60	2007
amiodarone	small molecule	nano Si	None	no matrix	65	2015
amoxicillin	small molecule	SiNP	None	no matrix	59	2012
amphetamine	small molecule	pSi	Derivatization	no matrix	26	2015
angiotensin	peptide	pSi	None	no matrix	23	1999
angiotensin	small molecule	pSi	None	no matrix	50	2017
angiotensin I	peptide	pSi	Derivatization	CHCA or SA	31	2006
angiotensin I	peptide	pSi	Functionalization	CHCA	28	2011
angiotensin I	peptide	nano Si	Derivatization	no matrix	72	2010
angiotensin I	peptide	nano Si	Derivatization	no matrix	75	2014
angiotensin I	peptide	nano Si	Derivatization	no matrix	76	2011
angiotensin I	peptide	pSi	None	DHB	47	2016
angiotensin I	peptide	nano Si	None	no matrix	70	2006

1	angiotensin II	peptide	SiNP	Functionalization	CHCA	56	2010
2	angiotensin II	peptide	nano Si	Derivatization	no matrix	75	2014
3	Angiotensin II	peptide	SiNP	None	CHCA	58	2010
4	angiotensin II (DRVYIHPF)	peptide	SiNP	Derivatization and functionalization	CHCA	55	2010
5							
6	angiotensin II (DRVYIHPF)	peptide	SiNP	Derivatization	no matrix	60	2007
7	angiotensin III	peptide	pSi	None	no matrix	30	2009
8	angiotensin III	peptide	pSi	None	DHB	47	2016
9	antiviral drug WIN	small molecule	pSi	None	no matrix	23	1999
10	Arachidic acid	small molecule	pSi	None	no matrix	24	2006
11	arachidonic acid	lipid	nano Si	Functionalization	no matrix	64	2016
12	arginine	small molecule	nano Si	None	no matrix	49	2016
13	arginine	small molecule	pSi	None	no matrix	50	2017
14	arginine	small molecule	pSi	None	no matrix	52	2008
15	arginine acids	small molecule	nano Si	None	CHCA	69	2013
16	Aspartic acid	small molecule	SiNP	None	no matrix	59	2012
17	Behenic acid	small molecule	pSi	None	no matrix	24	2006
18	Behentrimonium	small molecule	pSi	Functionalization	no matrix	41	2017
19	benzylpyridinium ions	small molecule	SiNW	Derivatization	no matrix	67	2006
20	beta-cyclodextrin	peptide	pSi	Functionalization	no matrix	48	2009
21	beta-lactoglobulin	protein	pSi	None	no matrix	21	2001
22	BNP	peptide	pSi	Derivatization and functionalization	CHCA	33	2008
23	bombesin	peptide	nano Si	Derivatization	no matrix	75	2014
24	bovine insulin	peptide	nano Si	None	no matrix	70	2006
25	bradykinin	peptide	pSi	None	no matrix	23	1999
26	Bradykinin	peptide	pSi	None	no matrix	29	2009
27	bradykinin	peptide	pSi	None	DHB	47	2016
28	Bradykinin	peptide	nano Si	None	no matrix	49	2016
29	bradykinin	small molecule	pSi	None	no matrix	50	2017
30	bradykinin	peptide	nano Si	None	CHCA	69	2013
31	bradykinin	peptide	nano Si	None	no matrix	77	2010
32	bradykinin 1-7	peptide	pSi	Derivatization	no matrix	22	2007
33	bradykinin 2-9	peptide	pSi	Derivatization	no matrix	22	2007
34	BSA	peptide	pSi	Derivatization	no matrix	22	2007
35	BSA	peptide	pSi	None	no matrix	21	2001
36	BSA	peptide	SiNW	Derivatization	no matrix	66	2005
37	BSA digest	peptide	SiNP	None	CHCA	58	2010
38	BSA digest	peptide	nano Si	None	no matrix	77	2010
39	Buprenorphine	small molecule	pSi	Derivatization	no matrix	43	2002
40	buprenorphine	small molecule	nano Si	None	no matrix	65	2015
41	butyrylcarnitine (C4)	small molecule	nano Si	None	no matrix	77	2010
42	caffeine	small molecule	pSi	None	no matrix	23	1999
43							
44							
45							
46							
47							
48							
49							
50							
51							
52							
53							
54							
55							
56							
57							
58							
59							
60							
61							
62							
63							
64							
65							

1	calcitonin	peptide	pSi	Derivatization	CHCA or SA	31	2006
2							
3	carnitine (C1)	small molecule	nano Si	None	no matrix	77	2010
4	cellobiose-probe	peptide	nano Si	None	no matrix	51	2017
5	cellotriase-probe	peptide	nano Si	None	no matrix	51	2017
6							
7	chlorpheniramine	small molecule	nano Si	None	no matrix	65	2015
8	Cholesterol	lipid	pSi	Functionalization	no matrix	41	2017
9							
10	Cholesterol	small molecule	pSi	Functionalization	no matrix	42	2010
11	cholesterol	small molecule	pSi	Functionalization	no matrix	48	2009
12	cholesterol	small molecule	pSi	Functionalization	no matrix	48	2009
13	cholesterol	small molecule	pSi	Functionalization	no matrix	48	2009
14	cholesterol	small molecule	pSi	Functionalization	no matrix	48	2009
15	cholesterol	lipid	pSi	Derivatization	no matrix	26	2015
16	choline	small molecule	pSi	None	no matrix	21	2001
17							
18	clonidine	small molecule	nano Si	Derivatization	no matrix	68	2008
19	clonidine	small molecule	nano Si	None	no matrix	65	2015
20							
21	Cocaine	small molecule	pSi	Derivatization	no matrix	32	2012
22	Cocaine	small molecule	pSi	Derivatization	no matrix	38	2015
23	Cocaine	small molecule	SiNW	Derivatization	no matrix	66	2005
24	codeine	small molecule	pSi	Derivatization	no matrix	22	2007
25	Codeine	small molecule	pSi	Derivatization	no matrix	26	2015
26							
27	corticosterone	small molecule	pSi	Functionalization	no matrix	48	2009
28							
29	cytochrome C	protein	SiNP	Derivatization and functionalization	CHCA	55	2010
30							
31	Dalargin	small molecule	pSi	None	no matrix	29	2009
32							
33	decanoylcarnitine (C6)	small molecule	nano Si	None	no matrix	77	2010
34							
35	Des-Arg1-Bradykinin	peptide	pSi	Derivatization	no matrix	43	2002
36	des-Arg9 Bradykinin	peptide	nano Si	None	no matrix	74	2011
37	des-Arg9-bradykinin	peptide	pSi	Derivatization	no matrix	34	2004
38	des-Arg9-bradykinin	peptide	SiNW	Derivatization	no matrix	66	2005
39	Des-Arg-bradykinin	peptide	nano Si	Derivatization	no matrix	72	2010
40	Des-Arg-Bradykinin	peptide	nano Si	Derivatization	no matrix	76	2011
41							
42	des-arg-bradykinin	peptide	pSi	None	no matrix	23	1999
43							
44	dextromethorphan	small molecule	nano Si	None	no matrix	51	2017
45							
46	diacylglycerol	lipid	nano Si	Functionalization	no matrix	64	2016
47							
48	dibutylphosphoric acid	small molecule	SiNP	Derivatization	no matrix	60	2007
49	Dichloromethyl phosphonate	small molecule	pSi	Derivatization	no matrix	43	2002
50							
51	Dichloromethylene bisphosphonate	small molecule	pSi	Derivatization	no matrix	43	2002
52							
53	diglycerides	lipid	SiNW	Functionalization	no matrix	63	2010
54							
55	ds-DNA	oligonucleotides	SiNP	Functionalization	3-HPA	62	2009
56	DTDMA C16/C16	small molecule	pSi	Functionalization	no matrix	41	2017
57	DTDMA C16/C18	small molecule	pSi	Functionalization	no matrix	41	2017
58	DTDMA C18/C18	small molecule	pSi	Functionalization	no matrix	41	2017
59							
60	EDDP	small molecule	pSi	Derivatization	no matrix	26	2015
61							
62							
63							
64							
65							

EDDP	small molecule	nano Si	Derivatization	no matrix	75	2014
erythromycin	small molecule	SiNP	None	no matrix	59	2012
fatty acids and glyceride	small molecule	SiNW	Functionalization	no matrix	63	2010
fentanyl	small molecule	nano Si	None	no matrix	65	2015
fentanyl	small molecule	nano Si	None	no matrix	77	2010
FHV	protein	pSi	None	no matrix	21	2001
FHV tryptic digests	protein	SiNW	Derivatization	no matrix	66	2005
fibrinopeptide B	peptide	nano Si	Derivatization	no matrix	72	2010
fibrinopeptide B	peptide	nano Si	Derivatization	no matrix	76	2011
Flunitrazepam	small molecule	pSi	Derivatization	no matrix	38	2015
four-residue peptide (MRFA)	peptide	pSi	None	no matrix	23	1999
glucose	small molecule	pSi	Functionalization	no matrix	48	2009
glucose	small molecule	pSi	Functionalization	no matrix	48	2009
glucose	small molecule	nano Si	None	no matrix	69	2013
glucose	small molecule	nano Si	Derivatization and functionalization	no matrix	71	2015
glucose	small molecule	nano Si	Derivatization and functionalization	no matrix	71	2015
glucose-probe	peptide	nano Si	None	no matrix	51	2017
glutamic acid	small molecule	pSi	Derivatization	no matrix	34	2004
glutamine	small molecule	pSi	None	no matrix	52	2008
glycine	small molecule	pSi	None	no matrix	52	2008
GSH	small molecule	pSi	Functionalization	no matrix	46	2017
GSH	small molecule	pSi	Functionalization	no matrix	46	2017
haloperidol	small molecule	nano Si	Derivatization	no matrix	68	2008
Heneicosanoic acid	small molecule	pSi	None	no matrix	24	2006
Heptadecanoic acid	small molecule	pSi	None	no matrix	24	2006
histidine	small molecule	pSi	None	no matrix	52	2008
insulin	peptide	pSi	Functionalization	CHCA	45	2014
insulin	peptide	SiNP	Functionalization	CHCA	57	2015
insulin B	peptide	pSi	None	no matrix	50	2017
isoleucine/leucine	small molecule	pSi	Derivatization	no matrix	34	2004
ketoconazol	small molecule	nano Si	Derivatization	no matrix	68	2008
L-cysteine	small molecule	pSi	Functionalization	no matrix	46	2017
Leu-Enkephalin-Arg	peptide	pSi	Derivatization	no matrix	43	2002
linoleic acid	lipid	nano Si	Functionalization	no matrix	64	2016
lipid species	lipid	pSi	None	DHB	47	2016
maltoheptaose	peptide	pSi	Functionalization	no matrix	48	2009
maltohexaose	peptide	pSi	Functionalization	no matrix	48	2009
maltotriose	small molecule	pSi	Functionalization	no matrix	48	2009
maltotriose	small molecule	pSi	Derivatization	no matrix	34	2004
MDMA	small molecule	pSi	Derivatization	no matrix	32	2012
MDMA	small molecule	pSi	Derivatization	no matrix	38	2015
methadone	small molecule	pSi	Derivatization	no matrix	26	2015

1	Methadone	small molecule	pSi	Derivatization	no matrix	37	2017
2	Methadone	small molecule	pSi	Derivatization	no matrix	37	2017
3	Methadone	small molecule	pSi	Derivatization	no matrix	37	2017
4	Methadone	small molecule	pSi	Derivatization	no matrix	38	2015
5	methadone	small molecule	nano Si	Derivatization	no matrix	75	2014
6	methamphetamine	small molecule	pSi	Derivatization	no matrix	26	2015
7	methamphetamine	small molecule	pSi	Derivatization	no matrix	32	2012
8	methionine	small molecule	pSi	None	no matrix	52	2008
9	metoprolol	small molecule	nano Si	None	no matrix	65	2015
10	Midazolam	small molecule	pSi	Derivatization	no matrix	43	2002
11	Midazolam	small molecule	pSi	Derivatization	no matrix	34	2004
12	midazolam	small molecule	SiNW	Derivatization	no matrix	66	2005
13	model sample of HRP digest and BSA	peptide	pSi	Functionalization	CHCA	45	2014
14	morphine	small molecule	SiNP	Derivatization	no matrix	60	2007
15	Murexine	small molecule	pSi	Derivatization	no matrix	36	2015
16	MYO digest	peptide	SiNP	None	CHCA	58	2010
17	myristoylcarnitine (C9)	small molecule	nano Si	None	no matrix	77	2010
18	N-(4-hydroxyphenyl)acetamide	small molecule	SiNP	None	no matrix	59	2012
19	neurotensin	peptide	pSi	Derivatization	no matrix	22	2007
20	neurotensin	peptide	nano Si	Derivatization	no matrix	72	2010
21	neurotensin	peptide	nano Si	Derivatization	no matrix	76	2011
22	neurotensin	peptide	pSi	None	no matrix	50	2017
23	nicotine	small molecule	pSi	Derivatization	no matrix	26	2015
24	N-octyl beta-D-glucopyranoside	peptide	pSi	None	no matrix	23	1999
25	Nonadecanoic acid	small molecule	pSi	None	no matrix	24	2006
26	nonanoic acid	lipid	pSi	Derivatization	no matrix	26	2015
27	norbuprenorphine	small molecule	nano Si	None	no matrix	65	2015
28	nordiazepam	small molecule	nano Si	None	no matrix	65	2015
29	norfloxacin	small molecule	SiNP	None	no matrix	59	2012
30	nucleobase adenine	peptide	SiNP	Derivatization	no matrix	60	2007
31	octanoylcarnitine (C5)	small molecule	nano Si	None	no matrix	77	2010
32	oleic acid	lipid	pSi	Functionalization	no matrix	41	2017
33	oleic acid	lipid	nano Si	Functionalization	no matrix	64	2016
34	Oxycodone	small molecule	pSi	Derivatization	no matrix	38	2015
35	Oxycodone	small molecule	pSi	Derivatization	no matrix	38	2015
36	Oxytocin	peptide	pSi	Functionalization	no matrix	40	2009
37	palmitoylcarnitine	small molecule	nano Si	None	no matrix	49	2016
38	palmitoylcarnitine	small molecule	pSi	None	no matrix	50	2017
39	palmitoylcarnitine (C10)	small molecule	nano Si	None	no matrix	77	2010
40	papaverine	small molecule	nano Si	Derivatization	no matrix	68	2008
41	PC head group	lipid	pSi	Functionalization	no matrix	41	2017
42	PEG	polymer	nano Si	None	DHB	69	2013
43	PEG 2300	polymer	pSi	Functionalization	no matrix	40	2009

PEG 400	polymer	pSi	Functionalization	no matrix	40	2009
PEG1000	polymer	SiNP	None	no matrix	59	2012
PEG400	polymer	nano Si	None	no matrix	70	2006
peptide mixture	peptide	SiNP	None	no matrix	54	2012
peptides from human serum and urine	peptide	SiNP	Functionalization	CHCA	56	2010
peptides leucine enkephalin	peptide	SiNP	Derivatization	no matrix	60	2007
Phenylalanine	small molecule	pSi	Derivatization	no matrix	34	2004
phosphatidylcholine	lipid	pSi	Derivatization	no matrix	22	2007
phosphatidylethanolamine	lipid	pSi	Derivatization	no matrix	22	2007
phospholipids	lipid	pSi	Derivatization	no matrix	22	2007
phosphopeptides	peptide	pSi	Derivatization and functionalization	DHB	39	2006
PPG1000	polymer	nano Si	None	no matrix	70	2006
prazosin	small molecule	nano Si	Derivatization	no matrix	68	2008
Prednisolone	small molecule	pSi	None	no matrix	29	2009
prednisone	small molecule	pSi	Functionalization	no matrix	48	2009
progesterone	small molecule	pSi	Functionalization	no matrix	48	2009
Pro-Leu-Gly tripeptide	peptide	nano Si	None	no matrix	77	2010
Propafenone	small molecule	pSi	Derivatization	no matrix	34	2004
propafenone	small molecule	SiNP	Derivatization	no matrix	60	2007
propafenone	small molecule	SiNP	Derivatization	no matrix	60	2007
propafenone	small molecule	SiNW	Derivatization	no matrix	66	2005
propranolol	small molecule	nano Si	Derivatization	no matrix	68	2008
Propranolol	small molecule	pSi	Derivatization	no matrix	43	2002
Psilocin	small molecule	pSi	Derivatization	no matrix	43	2002
quinidine	small molecule	nano Si	Derivatization	no matrix	68	2008
renin substrate tetrapeptide	peptide	pSi	Derivatization	CHCA or SA	31	2006
reserpine	small molecule	pSi	None	no matrix	23	1999
ropivacaine	small molecule	nano Si	None	no matrix	65	2015
roxithromycin	small molecule	SiNP	None	no matrix	59	2012
serum peptides	peptide	pSi	Functionalization	CHCA	45	2014
somatostatin 28	peptide	nano Si	Derivatization	no matrix	75	2014
spermidine	small molecule	nano Si	None	no matrix	49	2016
squalene	lipid	nano Si	Functionalization	no matrix	64	2016
ss-DNA	oligonucleotides	SiNP	Functionalization	3-HPA	62	2009
STAL-2 (hexapeptide, SFLLRN-NH2)	peptide	nano Si	None	no matrix	49	2016
stearic acid	lipid	pSi	Functionalization	no matrix	41	2017
Stearic acid	small molecule	pSi	None	no matrix	24	2006
stearoylcarnitine (C11)	small molecule	nano Si	None	no matrix	77	2010
streptomycin	small molecule	pSi	None	no matrix	50	2017

substance P	peptide	pSi	Derivatization	CHCA or SA	31	2006
substance P	peptide	nano Si	Derivatization	no matrix	75	2014
Substance P	peptide	pSi	Derivatization	no matrix	43	2002
sucrose	small molecule	pSi	Functionalization	no matrix	48	2009
sucrose	small molecule	pSi	Functionalization	no matrix	48	2009
sucrose	small molecule	pSi	Derivatization	no matrix	34	2004
Sutent	small molecule	nano Si	Derivatization	no matrix	72	2010
TAG 48:1	lipid	pSi	Functionalization	no matrix	41	2017
temporin-SHf	peptide	SiNP	None	no matrix	59	2012
testosterone	small molecule	pSi	Functionalization	no matrix	48	2009
TMZ	small molecule	nano Si	None	no matrix	69	2013
TPyP	small molecule	pSi	Functionalization	no matrix	40	2009
trans-androsterone	small molecule	pSi	Functionalization	no matrix	48	2009
trioctylamine	small molecule	SiNP	Derivatization	no matrix	60	2007
tripalmitin	lipid	SiNW	Functionalization	no matrix	63	2010
tristearin	lipid	SiNW	Functionalization	no matrix	63	2010
Trx-urodilatin	protein	pSi	Derivatization and functionalization	SA	27	2009
tryptic BSA digest	peptide	SiNP	Functionalization	CHCA	56	2010
tryptic peptide of protein fibronectin	peptide	pSi	Derivatization and functionalization	CHCA	44	2012
tryptophan	small molecule	pSi	None	no matrix	52	2008
Tyrian purple	small molecule	pSi	Functionalization	no matrix	41	2017
Tyrian purple	small molecule	pSi	Derivatization	no matrix	36	2015
tyrindoleninone	small molecule	pSi	Derivatization	no matrix	36	2015
tyrindoxyl hydrogen sulfate	small molecule	pSi	Derivatization	no matrix	36	2015
Tyrindoxyl sulfate	small molecule	pSi	Derivatization	no matrix	35	2012
verapamil	small molecule	nano Si	Derivatization	no matrix	68	2008
verapamil	small molecule	pSi	Derivatization	no matrix	22	2007
verapamil	small molecule	pSi	Derivatization	no matrix	34	2004
verapamil	small molecule	SiNP	Derivatization	no matrix	60	2007
verapamil	small molecule	SiNW	Derivatization	no matrix	66	2005
verapamil	small molecule	nano Si	None	no matrix	49	2016
verapamil	small molecule	nano Si	None	no matrix	65	2015
verapamil	small molecule	nano Si	Derivatization	no matrix	72	2010
vitamin D3	small molecule	pSi	Functionalization	no matrix	48	2009
WE 36:1	small molecule	pSi	Functionalization	no matrix	41	2017
γ -cyclodextrin	peptide	pSi	Functionalization	no matrix	48	2009